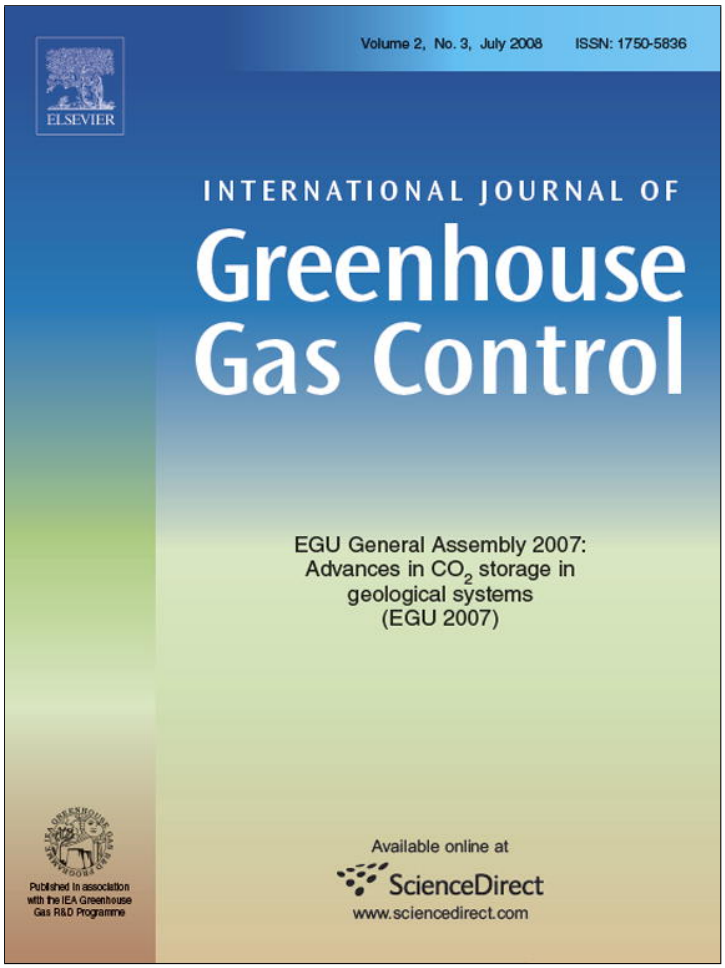

INTERNATIONAL JOURNAL OF GREENHOUSE GAS CONTROL 2 (2008) 353–372

available at www.sciencedirect.com

ScienceDirect

journal homepage: www.elsevier.com/locate/ijggc

Gas migration along fault systems and through the vadose zone in the Latera caldera (central Italy): Implications for CO_2 geological storage

*A. Annunziatellis, S.E. Beaubien *, S. Bigi, G. Ciotoli, M. Coltella, S. Lombardi*

Dipartimento di Scienze della Terra, Università di Roma "La Sapienza", Rome, Italy

ARTICLE INFO

Article history:
Received 16 July 2007
Received in revised form
4 February 2008
Accepted 7 February 2008
Published on line 2 April 2008

Keywords:
Gas migration
Faults
CO_2 geological storage
Natural analogue
Soil gas

ABSTRACT

A clear and detailed understanding of gas migration mechanisms from depth to ground surface is fundamental to choose the best locations for CO_2 geological storage sites, to engineer them so that they do not leak, and to select the most appropriate monitoring strategy and tools to guarantee public safety. Natural test sites (or "natural analogues") provide the best opportunity to study migration mechanisms, as they incorporate such issues as scale, long-time system evolution, and interacting variables that cannot be adequately addressed with laboratory studies or computer models. To this end the present work examines the migration to surface of deep, naturally produced CO_2 along various buried and exposed faults in the Latera caldera (central Italy) by integrating structural geology and near-surface gas geochemistry surveys. Results show how gas migration is channelled along discrete, high-permeability pathways within the faults, with release typically occurring from spatially restricted gas vents. Size, distribution, and strength of these vents appear to be controlled by the evolution and deformation style of the fault, which is in turn linked to the rheology of the lithological units cut by the fault. As such gas migration can change drastically along strike. Gas migration in the vadose zone around these vents is also discussed, focussing on how the physical–chemical characteristics of various species (CO_2, CH_4, and He) control their spatial distribution and eventual release to the atmosphere.

1. Introduction

Research conducted over the last 20 years indicates that the geological storage of anthropogenic CO_2, together with other approaches, is a technically viable option that can help reduce anthropogenic greenhouse gas loading to the atmosphere (IPCC, 2005, 2007). While confidence in CO_2 geological storage is given by the limited number of documented leakages at long-standing sites for CO_2 enhanced oil recovery, acid gas disposal, and natural gas storage (Lewicki et al., 2007a and references therein), and by the positive results obtained from highly monitored CO_2 injection sites like Sleipner (e.g. Chadwick et al., 2006) and Weyburn (Wilson and Monea, 2004), research into specific topics is still needed to ensure the efficiency and safety of this approach.

It is generally agreed that if leakage were to occur from a CO_2 geological storage site the main migration pathways would be along compromised boreholes or gas permeable

* *Corresponding author at*: c/o Prof. Salvatore Lombardi, Dipartimento di Scienze della Terra, Università di Roma "La Sapienza", Piazzale Aldo Moro, 5, 00185 Rome, Italy. Tel.: +39 06 49914918/+39 06 49914919.
E-mail addresses: stanley.beaubien@uniroma1.it, stanbeaubien@yahoo.it (S.E. Beaubien).
1750-5836/$ – see front matter
doi:10.1016/j.ijggc.2008.02.003

faults. Whereas the study of industrial sites is needed to better understand the former, natural analogues can be examined to address issues related to the latter. This has been well illustrated by various recent articles (e.g. Baines and Worden, 2004; Beaubien et al., 2005; Holloway et al., 2007; Lewicki et al., 2007a; Pearce, 2004, 2006) that review and compare the results of natural analogues studies as applied to CO_2 geological storage.

Natural analogue sites can be broadly divided into two end-members, those that do not leak and those that do. While well-sealed, natural CO_2 reservoirs can help us to understand the processes that isolate CO_2, and other gases, in the subsurface (e.g. Brennan et al., 2004; Gaus et al., 2004; Le Nindre et al., 2006; Stevens et al., 2004), it is the leaking CO_2 reservoirs that can be used to study fault-controlled gas migration. These sites, many of which have been leaking CO_2 for hundreds to thousands of years, can be used to address the questions of scale, time, structural and chemical evolution, and natural complexity that cannot be adequately considered in laboratory experiments or computer models.

Large-scale gas leakage in natural systems occurs most commonly in volcanic or geothermal areas, where magma degassing or thermo-metamorphic alteration of carbonates results in the production of large volumes of CO_2. The common occurrence of deep faults associated with these features then provides a permeable pathway along which this CO_2 can migrate towards the atmosphere. A large number of studies have been conducted on these leaking natural analogues to assess the impact of CO_2 on water quality (Wang and Jaffe, 2004), mineral alteration (Stephens and Hering, 2002), and plant and ecosystem health (Pfanz et al., 2007), to quantify the risk to humans associated with the gas released from these structures (Beaubien et al., 2003), and to test innovative monitoring technologies (Anderson and Farrar, 2001). By far most of the papers have been written, however, on the study of the origin, distribution, controlling mechanisms, and mass transfer rates of deep gas to the atmosphere at such well-studied sites as Mammoth Mountain, USA (Gerlach et al., 2001; Lewicki et al., 2007b), Long Valley, USA (Bergfeld et al., 2006), and the Albani Hills, Italy (Chiodini and Frondini, 2001), to name just a few.

Although many of these papers are put in the context of the structural setting of the area, few are focused directly on the relationship between gas release and the faults and fractures that provide the conduits for upward migration. This approach is more commonly found where soil gas surveys have been specifically conducted across such features (e.g. Azzaro et al., 1998; Baubron et al., 2002; Ciotoli et al., 2007; Fountain and Jacobi, 2000; King et al., 1996; Lewicki and Brantley, 2000; Lewicki et al., 2003), although the gas migration rates in these studies are typically much lower than that observed above geothermal areas. Studies like these have highlighted the irregular distribution of gas migration along strike, likely due to channelled flow of deep gases along more permeable intervals of the fault and their subsequent release at surface within localised areas aligned along the fault trace.

The issue of fluid movement along faults has also been studied extensively from a structural point of view to better understand the influence of fluids on fault movement and how fault evolution can, in turn, control fluid migration. For example, studies have shown how: (i) fault zones can act as barriers, conduits, or mixed conduit–barrier systems (Antonellini et al., 1994; Caine et al., 1996; Evans et al., 1997; Sibson, 2000); (ii) structural and hydraulic properties can vary over time and space as a fault evolves (Gibson, 1994; Tellam, 1995; Wibberley and Shimamoto, 2003); (iii) local- and regional-scale permeability anisotropy can be related to different stages of deformation evolution (e.g. Agosta and Aydin, 2006; Caine and Forster, 1999; Haynekamp et al., 1999); and (iv) active faults can trigger gas leakage by increasing rock and soil permeability (Uehara and Shimamoto, 2004). Fault permeability models have also been proposed for faults in clastic, crystalline, and, more recently, for carbonate rocks (Agosta and Aydin, 2006; Antonellini et al., 1994; Barton et al., 1995; Bruhn et al., 1994; Caine and Forster, 1999; Flodin et al., 2005; Rawling et al., 2001; Sholtz, 1987), although less exists for volcanic terrains (e.g. Gray et al., 2005). Fault permeability has particularly been linked to the lithology of the faulted rocks (Morrow et al., 1984; Zhang and Cox, 2000; Zhang and Tullis, 1998; Zhu and Wong, 1997, 1999; Zoback and Byerlee, 1975).

It is generally accepted that fault zones consist of two main compartments, a central core surrounded by lateral damage zones (Antonellini et al., 1994; Caine et al., 1996; Chester et al., 1993). The fault core is the interval in which various mechanical and chemical processes have destroyed the fabric of the host rock (Chester and Logan, 1986; Sibson, 1977), while the damage zone consists of a wider interval of fractures and smaller faults where the primary fabric is still visible (Cowie and Scholz, 1992). These compartments are then surrounded by weakly deformed host rocks. The thickness of the damage and core zones can vary along a fault plane and, with them, their hydraulic properties (Caine et al., 1996; Evans et al., 1997). Structural assemblage changes have also been studied as a function of offset variation and distribution along strike (Sholtz, 1987), which is connected to fault growth and the linkage of initially separate fault planes (Morley and Wonganan, 2000, among many others).

The Latera caldera, located in central Italy (Figs. 1 and 2), is an example of a highly faulted, leaking, natural analogue site. Over the last few years the area above this geothermal field has been studied extensively to better understand the migration, impact, and potential for detection of leaking deep CO_2 (Bateson et al., 2008; Beaubien et al., 2008; Chiodini et al., 2007; Lombardi et al., 2006, 2008; Pettinelli et al., 2008). The present study has used this site to examine how various fault features (such as fault geometry, size, and evolution) influence the migration behaviour of CO_2, as well as the processes in the vadose zone that control the eventual transfer of gas to the atmosphere. Field work involved the close integration of structural geology and near-surface gas geochemistry surveys, as well as examination of historical borehole logs for deep wells (up to 3000 m) drilled in the 1970s for geothermal exploration.

2. Geological and structural setting of the Latera caldera

The geology of the west-central Italian peninsula can be thought of as the product of two main tectonic events, a

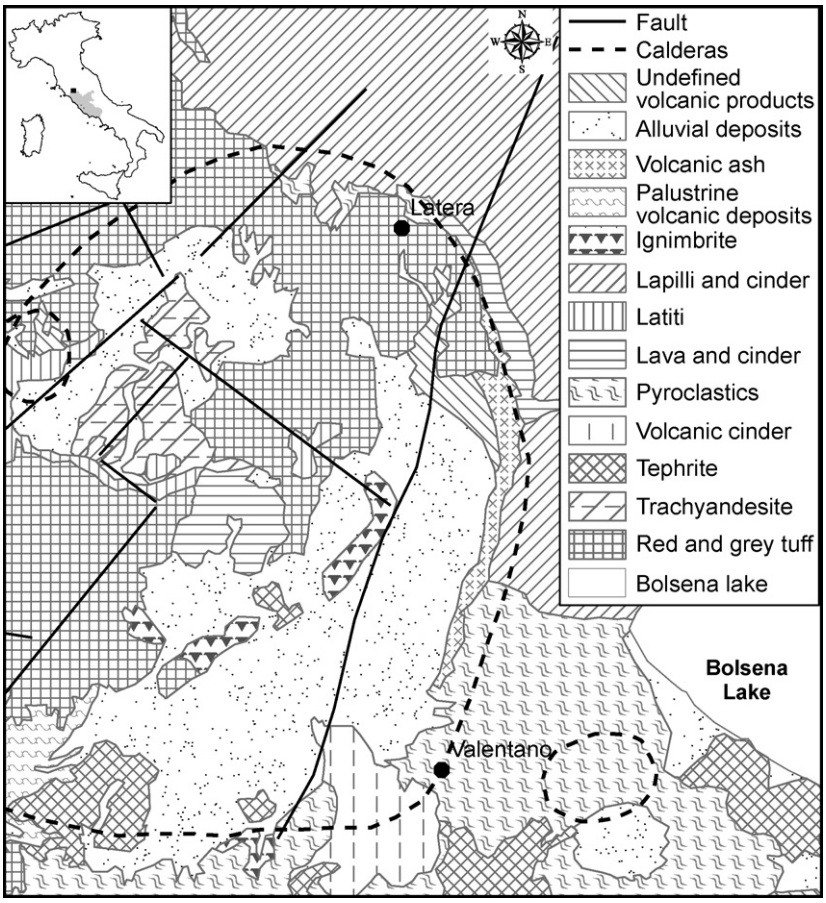

Fig. 1 – Geological map of the Latera caldera.

compressive phase during the Eocene to Late Miocene and a subsequent extensional phase from the Late Miocene through the Quaternary (Carmignani and Kligfield, 1990).

The regional substratum of this area consists of metamorphic phyllites and micaschists (see Appendix A for more details), onto which a series of ''tectonic units'' were placed during the initial compressive period via thrusts that trend primarily N–S. In the area of the Latera caldera, and throughout central Italy, these units are mainly formed by the Mesozoic ''Tuscan nappe'' and the Cretaceous to Eocene ''Ligurian flysch'' (Fig. 3). The Tuscan nappe consists primarily of carbonates and some siliciclastic successions; because of high secondary permeability in the carbonates, this unit forms a regional aquifer and locally hosts the geothermal reservoir beneath the Latera caldera. The overlying Ligurian flysch is made up of various units, including impermeable shales and siltstones which act as a regional aquitard and which locally form the caprock for the geothermal reservoir and associated CO_2.

The subsequent extensional regime, which was related to the opening of the Tyrrhenian Sea, resulted in the formation of a series of NW-SE to N–S trending grabens and normal fault systems which dissected the previous compressional fold and thrust belt (Di Filippo et al., 1999; Funiciello and Parotto, 1978). The extensional phase also caused crustal thinning, resulting in significant volcanic activity during the Quaternary. The Vulsini volcanic district was formed during this period, consisting of the three main eruptive centres of Latera (Fig. 1), Bolsena, and Montefiascone. Volcanism in this area began about 0.8 Ma ago (Evemden and Curtis, 1965; Nicoletti et al., 1979), with most of the Latera products being dated from 232 to 156 ka (Turbeville, 1992). More details regarding the local geology are given in Appendix A.

At the cessation of Latera volcanic activity, edifice collapse created the caldera via a series of associated normal faults which, combined with thrusts, regional normal faults, and extensive fracturing associated with the volcanic eruptions themselves, became conduits for upwardly migrating hydrothermal fluids and CO_2. Many of these conduits became sealed via secondary mineral precipitation (Cavarretta et al., 1985). This process has made much of the overlying flysch and volcanic units impervious, except where gas is locally escaping, and helped to partially isolate the underlying geothermal reservoir.

The reservoir itself is located within a structural high of Tuscan limestones (Barberi et al., 1984; Palladino and Simei, 2005) (Fig. 3), a feature which may represent a recumbent fold (Bertrami et al., 1984), an ancient caldera rim (Barberi et al., 1984), or a series of superimposed thrust sheets (this work). This structural high is bounded laterally by sealed faults and thermo-metamorphosed carbonates, below by the metamorphic basement, and above by low permeability Ligurian

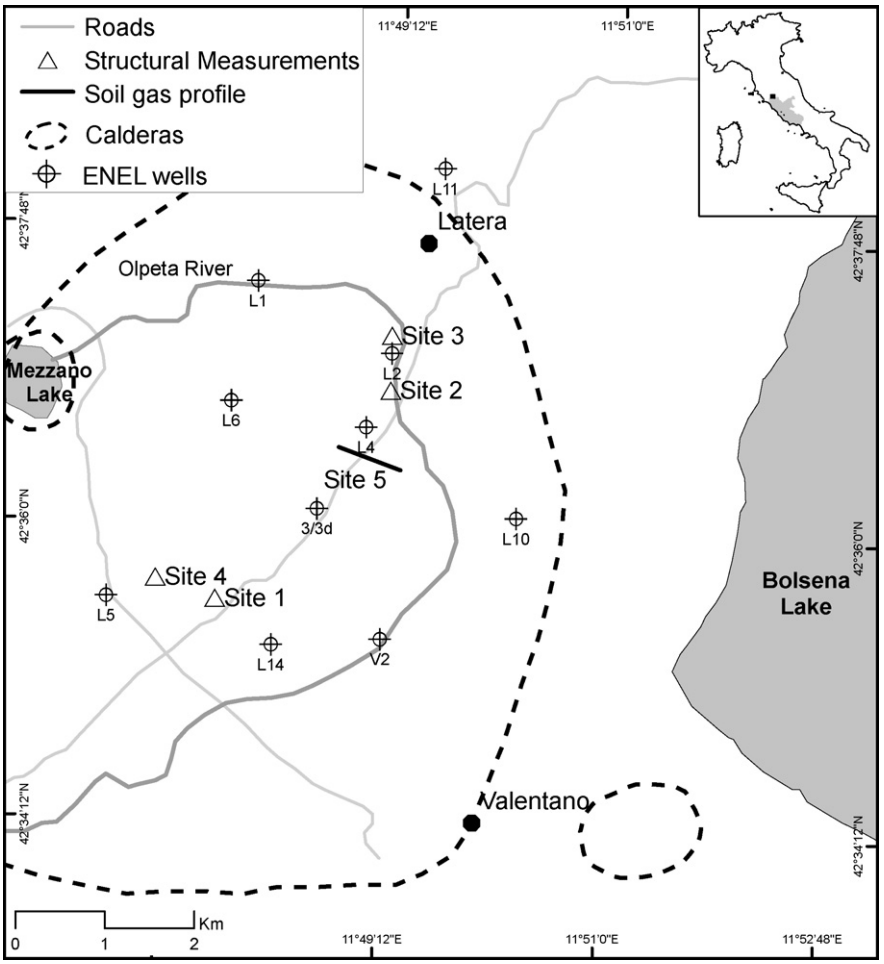

Fig. 2 – Map showing the four sites where structural measurements were made (sites 1–4) and the location of a detailed soil gas profile across a number of gas vents (site 5). Three of the sites (1, 3, and 4) are quarries that gave excellent exposure for structural measurements. The location of the deep geothermal exploration wells ("ENEL wells") is given for reference.

flysch and volcanic pyroclastics. The reservoir limestones are heavily fractured and folded, then locally re-sealed with a composite hydrothermal assemblage (Cavarretta et al., 1985). Maximum permeability within the reservoir occurs along the major, NNE–SSW-trending axis of the structure (Sabatelli and Mannari, 1995).

The CO_2 that leaks at the surface is likely the product of metamorphic alteration of the reservoir limestones, driven by the water-dominated system and the high heat flow (presently ranging from 170 to 230 °C) linked to the original magma intrusion (Chiodini et al., 1995; Duchi et al., 1992; Minissale, 2004), although a portion may also come from a deeper mantle component (Chiodini et al., 2007). Because the geothermal system is water-dominated the majority of gas samples collected from the deep wells are dissolved gases that exsolve at the lower pressures at surface. In general, most reservoir waters contain 3–6% "Non Condensable Gases" (NCG) (Sabatelli and Mannari, 1995), with well L2 (Fig. 2) having a representative composition of 98.35% CO_2, 0.05% CH_4, 1.22% H_2S, 0.4% N_2 and trace levels of H_2 (Bertrami et al., 1984). One well (L11; Fig. 2) did intersect a gas-only reservoir having 98% CO_2 (Lombardi et al., 1993). Based on calculations using total surface heat flux, enthalpy of liquid water at reservoir temperatures, and the CO_2 molality in the reservoir water, Gambardella et al. (2004) estimated a total CO_2 production rate of 2.58×10^8 mol CO_2 year^{-1} for the approximately 20 km^2 surface area of the reservoir.

At the surface the central part of the Latera caldera is characterised by a NE–SW to N–S trending hydrothermally altered area, with silica, alunite, and kaolinite formed in the vicinity of several gas vents and thermal/cold springs (Gianelli and Scandiffio, 1989; Lombardi and Mattias, 1987; Lombardi et al., 1993). These two directions have also been observed by Buonasorte et al. (1991) in a geomorphological study of the dominant morphological elements located throughout the Vulsini mountains.

3. Study site description

The Latera caldera, located about 110 km to the NW of Rome, Italy (Fig. 2), is a NE–SW trending elliptical depression consisting of a relatively flat central agricultural plain surrounded by tree-covered, 100 m high hills. Except for some

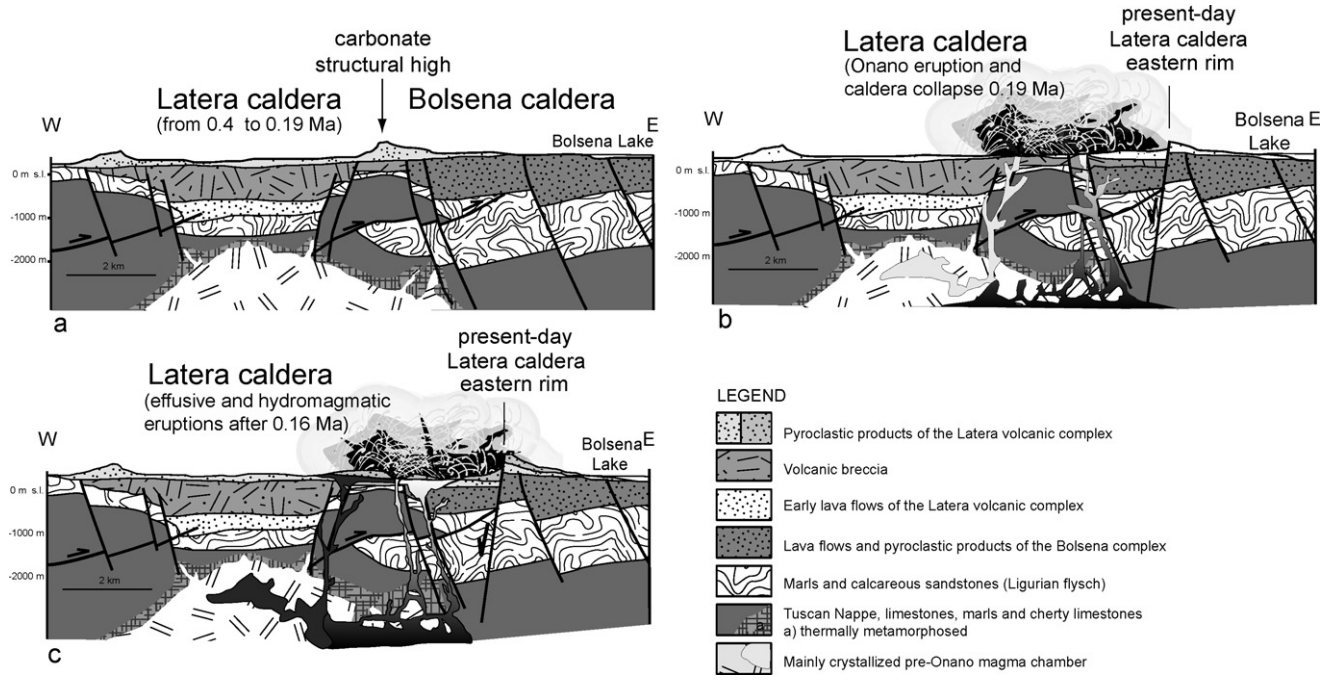

Fig. 3 – W–E schematic geological sections illustrating the main steps of the evolution of the Latera caldera; subsurface data after Barberi et al. (1984) and Palladino and Simei (2005). The individual figures refer to the main period of explosive activity from 0.4 to 0.2 Ma (a), the Onano eruption around 0.17 Ma (b), and hydromagmatic eruptions during the later stages of activity (c). See the text and Appendix A for details.

local hills formed by resistive volcanic units, the caldera plain is covered by tens of metres of alluvium.

In addition to a regional examination of the Latera caldera, five small sites were chosen for detailed work (Fig. 2); structural measurements were made at sites 1–4, CO_2 flux measurements were performed at site 3, and a horizontal profile of soil gas and CO_2 flux measurements was conducted at site 5. Site 1 is a large, presently active, open-pit kaolinite quarry which has 5–10 m high exposures on its south-western and south-eastern walls; the other two sides of the quarry are lower with poor exposure and extensive vegetation cover. Site 2 is a linear rock escarpment into which a series of caves have been dug; these caves have been blocked off by local authorities due to the accumulation of CO_2 and H_2S coming from fractures in the surrounding rock. Site 3 is an abandoned kaolinite and sulphur mine cut into a hillside; because of the extensive work conducted at this site it is described in more detail below. Site 4 is a very small exposure in thick forest that at one time was likely excavated for potential kaolinite extraction but never developed; the 3 m high exposure is cut into a large hill on the NE side. Finally, site 5 is located on the caldera plain. Here there is no exposure, but instead relatively flat agricultural fields are located on 10–50 m thick alluvial sediments that host an unconfined aquifer at about 4 m depth.

Site 3 was chosen for extensive structural and geochemical surveys due to the excellent exposure of a large fault structure. Quarrying into the hillside at this site created a ''U''-shaped feature having 2–10 m high quarry walls on three sides that surround a flat quarry floor. Three mine adits were originally dug into the south-western face of the quarry, first for sulphur until 1950 and then for kaolinite until its closure in the early 1970s. For safety reasons, the tunnel entrances were closed at this time with the same wall material. The fault, which is exposed on this south-western face, strikes across the flat quarry floor where a detailed gas flux survey was conducted. Interviews with ex-employees of the mine indicate that the tunnels went straight into the hillside (i.e. towards the southwest), and thus there should not be any man-made feature beneath the quarry floor (located to the north-east). The quarry floor is devoid of vegetation and covered with a thin (5–30 cm) layer of fine sediments, although the underlying fractured and altered volcanic rocks can be seen in some locations.

4. Methodology

4.1. *Analysis of brittle deformation*

A preliminary, regional analysis of faults and fractures was first carried out in the Latera caldera. Due to limited outcrop exposure, about 70 fracture and small fault measurements were collected in the four kaolinite and sulphur quarries described above (Fig. 2). All data have been projected on equi-areal Schmidt diagrams (lower hemisphere) and plotted on merged pole-to-plane and density diagrams.

4.2. *Soil gas geochemistry*

Soil gas samples were collected using a 6.4 mm diameter, thick-walled, stainless-steel probe pounded in the ground

with a co-axial hammer to a depth of about 60–80 cm to avoid the influence of atmospheric air (Hinkle, 1994). All soil gas surveys were conducted during low-precipitation seasons (typically summer to early fall) to minimise any variations induced by different sampling periods. As such it is believed that all the surveys represent the same populations and that they can be combined for statistical and geo-spatial analysis.

Field analyses were conducted for carbon dioxide (CO_2), hydrogen sulphide (H_2S), and hydrogen (H_2) using a gas analyser (Draeger Multiwarn) connected directly to the probe. Samples were also collected from the probe for laboratory analysis by injecting 60 ml of soil gas into a previously evacuated, 25 ml stainless-steel container having a screw top port with a compressible septum. These containers were analysed in the laboratory first for helium (He) on a mass spectrometer (Varian Leak Detector) and then for other gases on two Fisons 8000-series bench gas chromatographs. These gases included CO_2, oxygen + argon (O_2 + Ar), nitrogen (N_2), methane (CH_4), and ethane (C_2H_6).

Two soil gas datasets are presented here. The first consists of a combined dataset formed by various regional (2 samples km^{-2}) and detailed (40–50 samples km^{-2}) soil gas surveys performed throughout the Latera caldera over the last number of years. The total number of sample points in this dataset depends on the gas type (He, 2467; CO_2, 1735; CH_4, 938). The second dataset is formed by 202 points sampled along a detailed, 550 m long horizontal profile crossing a number of gas vents (site 5, Fig. 2). Not all points were sampled for all parameters. Instead, sample spacing along the profile for the field analysis of soil gas CO_2 and CO_2 flux was 2–4 m, while it was 8–12 m for laboratory analysis of soil gas He and CH_4 in low CO_2 areas and every 4 m in anomalous CO_2 areas.

4.3. CO_2 flux geochemistry

Carbon dioxide flux measurements were made using a closed-circuit accumulation system (e.g. Hutchinson and Livingston, 1993) that was constructed "in-house". The control unit is equipped with a 0–3000 ppm infrared CO_2 detector while the accumulation chamber itself is a small Plexiglas box with an inlet and outlet tube for the IR detector and a 30 cm long, 5 mm diameter pressure equilibration tube to prevent artefacts above high flux points and on windy days (Hutchinson and Mosier, 1981). The accumulation chamber was pressed firmly to the ground to insure a proper seal after the removal of any surface vegetation, and CO_2 concentrations were measured and stored every second for about 100 s. Flux values were calculated using:

$$\phi CO_2 = \left(\frac{d[CO_2]}{dt}\right)\left(\frac{V}{A}\right)\left(\frac{T_0}{T}\right)\left(\frac{P}{P_0}\right)k \quad (1)$$

where $(d[CO_2]/dt)$ is the first linear slope of the CO_2 concentration increase (ppm/s), V is the chamber volume (m^3), A is the chamber surface area (m^2), T and T_0 are measured and standard temperature (°K), P and P_0 are measured and standard pressure (kPa), and k is a unit conversion factor (169.71).

A highly detailed grid of CO_2 flux measurements was performed on the floor of the site 3 quarry (Fig. 2) to understand the distribution of gas migration relative to the local structural features. Flux measurements were conducted on a regular grid covering a total area of 50 m × 70 m and having a sample spacing of 3 m × 5 m; samples were collected every 3 m along a series of parallel lines trending N350°E (i.e. perpendicular to the main fault direction) and located 5 m apart. Soil gas samples were not collected here due to the very shallow occurrence of solid rock. CO_2 flux measurements were also conducted at site 5 along the detailed horizontal profile described above.

4.4. Gas geochemistry data analysis

Preliminary data analysis involved the calculation of standard statistical parameters to evaluate the basic characteristics of the data, the creation of normal probability plots (NPP) to define statistical populations for each parameter and to choose contour thresholds, and the creation of post and classed post maps to analyse sample and value distribution.

A subsequent geostatistical study consisted of experimental variogram calculations to check spatial continuity of the data values and the presence of anisotropies. As geostatistical analyses provide poor results with non-normal sample distributions, the CO_2 flux and soil gas concentration data were log-transformed to obtain a normal distribution and to reduce the influence of outliers. Once the data spatial continuity was characterised it was modelled using variogram functions that formed the basis for contouring with the kriging method. Finally, cross-validation was used to validate the model parameters used for the estimation.

Collected data were processed using the following software: Grapher 6.0 and Surfer 8.0 (Golden Software, Inc.), Statistica 6.0 (StatSoft, Inc.), GS + (Gamma Design Software, LLC), and ArcGIS (ESRI, Inc.).

5. Results

5.1. Regional study

Surveys were conducted at the caldera scale to better understand the overall structural architecture of the area and how this controls the migration of gas to the surface.

5.1.1. Structural geology

Extensive structural measurements were collected at four sites located throughout the valley floor (Fig. 2). In general, fractures and fault systems observed at these locations vary locally from a very low density (about one fracture every 150 m) to higher values (about one fracture every 50 cm). Combined pole-to-plane and density plots (Fig. 4) of this data show clusters around N50°E and N10°E, which is in agreement with other measurements made by the authors on the caldera edge and rim.

Fractures belonging to the N50°E system have well-defined surfaces that are generally open and filled by shale. The opening is typically mode I (i.e. opening normal to the fracture walls), but several of these fractures belong to mode II, as shown by small pull-apart features along the planes that indicate a normal sense of shear. The N10°E fractures are mode I and are generally associated with fine breccias of a few

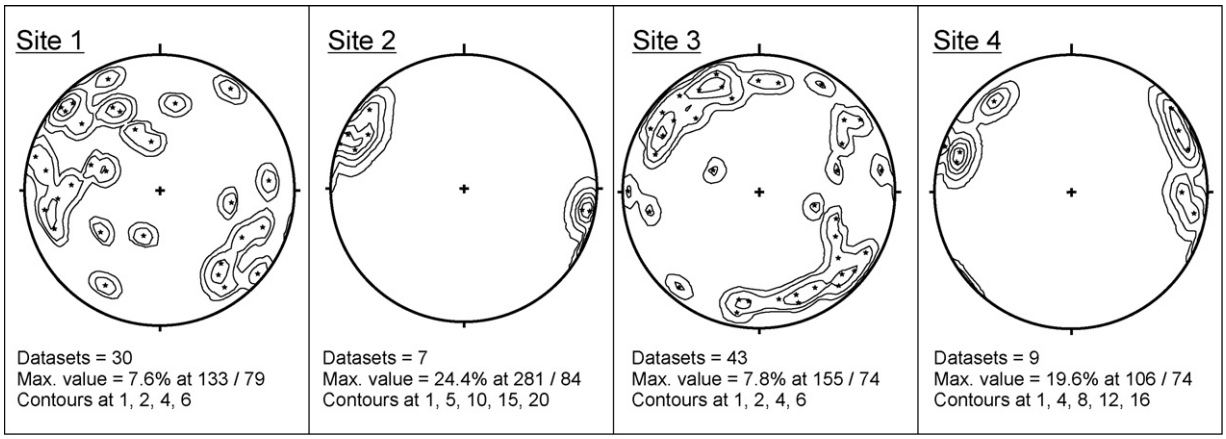

Fig. 4 – Fault pole and pole density plots of the faults and fractures measured at each site.

millimetres. Most of these fractures reach the field surface, with evidence of shallow fluid circulation (black to brown alteration and encrustations, irregular planes) (Fig. 5a).

Small faults have been measured in all the quarries. They have an offset of about 20–40 cm, strike from N20°E to N50°E (Fig. 5b and c), and most show evidence of active fluid circulation in the form of secondary sulphate minerals.

5.1.2. *Soil gas geochemistry*

As mentioned, a number of regional and detailed soil gas surveys throughout the Latera caldera were combined to compare soil gas trends with the results of the structural geology surveys described above. Table 1 summarises various statistical parameters for three gases (CO_2, CH_4, He) of this combined dataset and contrasts them with an Italian-wide dataset, created by the authors over the last 30 years of soil gas sampling, and a sub-set of just-volcanic areas. The combined Latera dataset shows a skewed distribution for CO_2 and CH_4, as indicated by the large difference between mean and median values and by the high standard deviation values (Table 1). In contrast the He distribution is primarily Gaussian, except for a few outliers. When compared with other volcanic areas, and the database as a whole, the Latera dataset has the highest mean and median CO_2 and CH_4 values, while He values are slightly lower.

Experimental variograms were calculated for the log-transformed Latera CO_2 dataset using the average distance between samples (about 200 m) as the starting lag. The resultant variogram surface maps (not shown) highlight the presence of two main anisotropy axes acting at different spatial scales and different directions: (i) a small-scale behaviour along a direction of N45°E, with a spatial range of 350 m along the major axis of anisotropy and 150 m along the minor axes of anisotropy; and (ii) a large-scale behaviour along

Table 1 – Soil gas statistics for the regional and detailed sites at Latera, compared to the statistics for a pan-Italian database produced by the authors over the last 30 years

	N	Mean	Median	Min	Max	LQ	UQ	0.10%	0.90%	IQR	S.D.
Latera regional study											
He (ppm)	2,467	5.35	5.29	4.24	9.86	5.17	5.42	5.01	5.62	0.25	0.45
CO_2 (%)	1,735	6.74	1.30	0.03	100.00	0.64	4.22	0.34	19.60	3.58	15.09
CH_4 (ppm)	938	26.40	1.09	0.11	1345.34	0.56	2.03	0.33	18.50	1.47	126.92
Sulphur quarry (site 3)											
CO_2 flux ($g\,m^{-2}\,d^{-1}$)	267	1700.28	331.52	7.02	49563.63	138.22	1050.27	47.11	3828.30	912.05	4992.67
Horizontal profile (site 5)											
He (ppm)	75	5.38	5.33	4.63	8.13	4.90	5.47	4.80	6.93	0.56	0.82
CO_2 (%)	82	17.68	8.70	0.42	85.92	3.20	19.51	1.47	52.35	16.30	2.38
CH_4 (ppm)	82	57.61	0.32	0.00	1019.04	0.16	0.65	0.16	4.41	0.49	218.37
CO_2 flux ($g\,m^{-2}\,d^{-1}$)	147	131.10	5.06	3.25	3569.73	9.05	55.78	5.70	210.26	46.72	426.43
Other Italian volcanic areas											
He (ppm)	15,080	5.45	5.33	1.20	172.96	5.22	5.48	5.04	5.70	0.26	2.29
CO_2 (%)	4,860	3.33	0.88	0.03	100.00	0.41	1.92	0.18	4.81	1.51	10.32
CH_4 (ppm)	3,395	16.61	1.69	0.01	7104.26	1.04	2.39	0.63	3.83	1.35	167.08
Complete Italian database											
He (ppm)	38,060	5.48	5.31	1.20	315.22	5.20	5.48	5.02	5.76	0.28	2.95
CO_2 (%)	16,301	1.93	0.83	0.03	100.00	0.38	1.69	0.16	3.22	1.31	6.09
CH_4 (ppm)	11,945	14.65	1.83	0.01	19396.14	1.16	2.54	0.72	3.41	1.38	263.10

Fig. 5 – Examples of faults and fractures from the Latera caldera area. (a) Fracture with an irregular plane in pyroclastic deposits at the site 1 quarry (Fig. 2); (b) high angle normal fault in lavas altered to kaolinite at the site 3 quarry; (c) small normal fault in pyroclastic deposits at the site 1 quarry.

a direction of N20°E, with a spatial range of 800 m along the major axis of anisotropy and of 300 m along the minor axes of anisotropy. These two directions are in good agreement with that observed in the structural results presented above. The resultant equation of the variogam model is $\gamma = 1.4$ Nugget + 1 Sph (350, 150, 45) + 0.6 Sph (800, 300, 20), which was used in the kriging calculations to interpolate/extrapolate values at unsampled locations. Furthermore, the calculation of the experimental variogram perpendicular to the large-scale anisotropy axis shows repetitive high and low spatial variance, indicating the presence of a phenomenon that repeats itself in space with a range of about 300 m.

The resultant contour map (Fig. 6) shows a number of elongated soil gas CO_2 anomalies that trend from N10°E to N50°E. Values above 2.5% (outlined with a black line). Values above 2.5% were considered anomalous based on the normal probability plot distribution of this dataset.

The results for the detailed profile conducted at site 5 across a number of gas vents in the centre of the Latera caldera are shown in Fig. 7, where soil gas CO_2, CH_4, and He are plotted together with CO_2 flux values. The trend of all four parameters is generally similar, with elevated values observed in the intervals from 0 to 50 m, 200 to 225 m, 300 to 360 m, and 400 to 500 m. These four venting features are well resolved with this detailed profile, compared to the large, ''spatially averaged'' anomalies that are observed in the regional map of Fig. 6. The sections between these vents clearly show background values that are not influenced by deep leaking CO_2; background values for the profile dataset, defined using normal probability plots, are: CO_2 flux $< 22\ g\ m^{-2}\ d^{-1}$; $[CO_2] < 2.5\%$; $[CH_4] < 1.5$ ppm; and [He] < 5.25 ppm. Although not shown, O_2 and N_2 distributions mirror exactly that of CO_2: $[O_2] = 20.44 - 0.203[CO_2]$ with $r^2 = 0.995$; $[N_2] = 77.35 - 0.756[CO_2]$ with $r^2 = 0.995$. This indi-

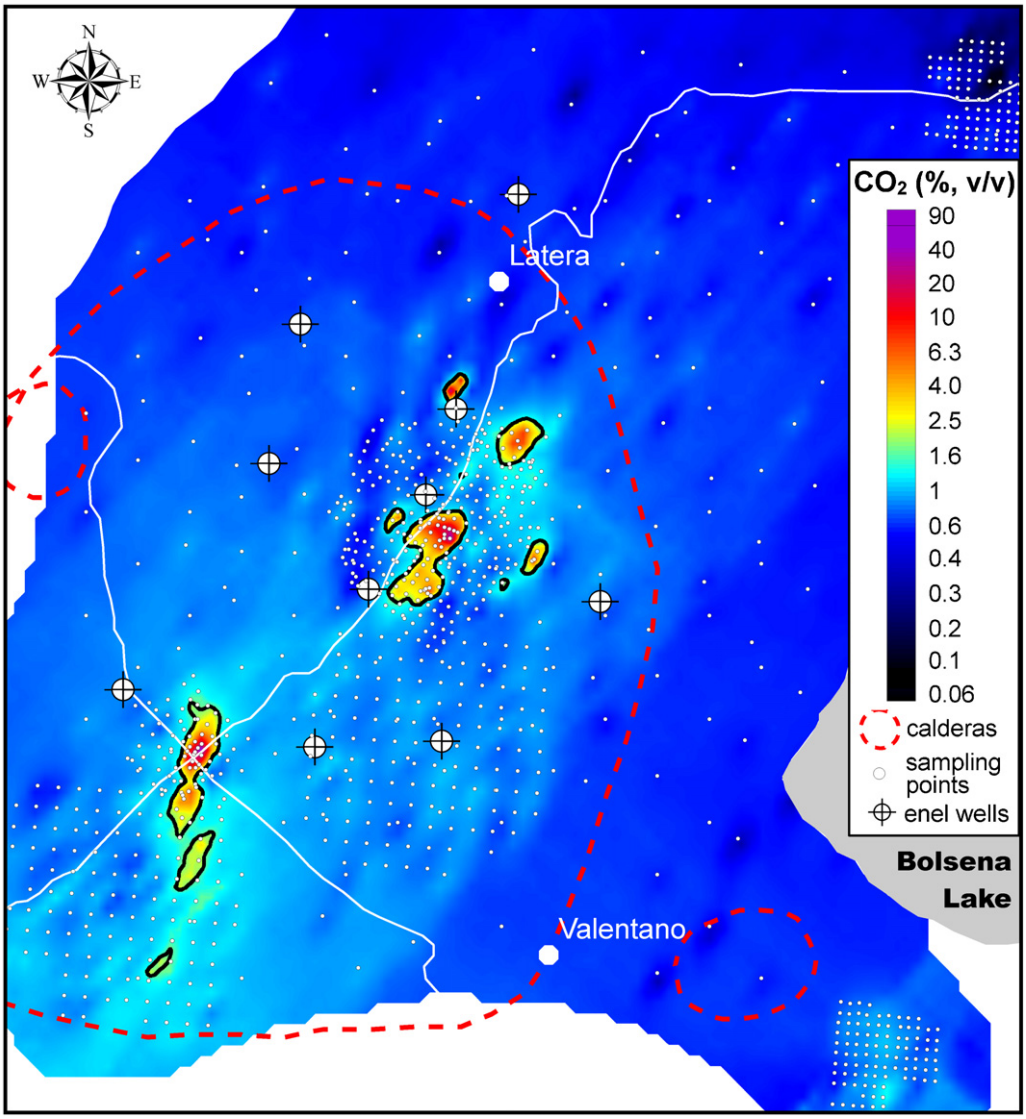

Fig. 6 – The contoured distribution of CO_2 soil gas concentrations throughout the Latera caldera area, with anomalous values above 2.5% CO_2 outlined in black. White dots show the sampling locations while the deep geothermal exploration wells are the same as given in Fig. 2.

cates progressive dilution of essentially atmospheric air in the soil pores by the deep CO_2.

5.2. *Detailed study*

The excellent exposure of a fault in the quarry wall of site 3 (Fig. 2) has allowed for highly detailed structural and CO_2 flux measurements, with the goal of understanding how small-scale structural features and fault evolution can control gas movement.

5.2.1. *Structural geology*

The site 3 quarry is located in what appears to be volcanic lava flows (based on primary textures) that have been almost completely altered to kaolinite. The quarry face extends for about 100 m and has two main directions: N20°W and N70°E. As in the other quarries the deformation is essentially brittle, consisting of small faults and fractures that cluster around the two main directions illustrated above (N10°E and N50°E; Fig. 4); where observable faults have mainly dip–slip kinematics with a generally normal sense of shear.

The distribution of structural elements along the face of the quarry is variable. In general, fractures and faults are concentrated in 5–6 m wide domains having high deformation density, separated by intermediate domains where the density is lower. These high density fracture domains can be subdivided into three main configurations, which we believe represent different stages of the normal faulting process and/or the distribution of deformation along strike (i.e. evolution in time and/or space). As discussed below, these different styles have a significant influence on the gas migration pathways.

The first style is referred to as "single fault plane" deformation, and it is usually located within low-density fracture domains where primary structures are still well

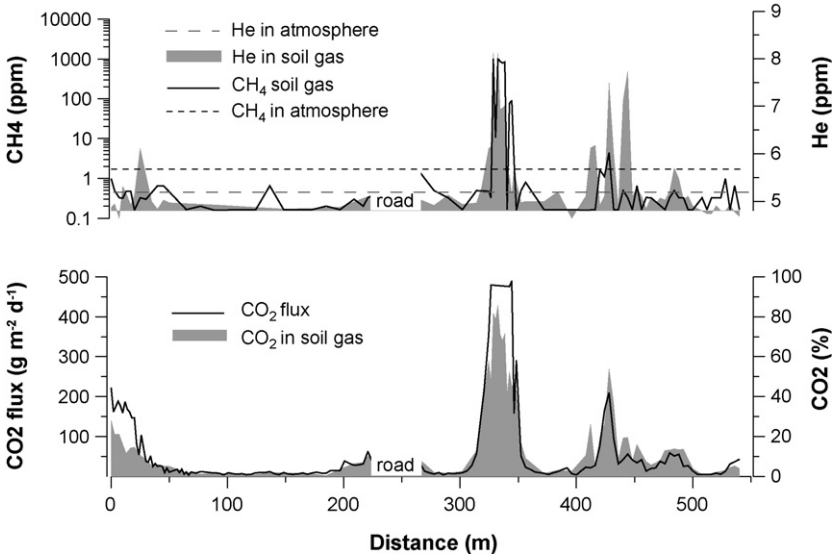

Fig. 7 – Site 5 gas geochemistry profile conducted across a number of gas vents in the centre of the Latera caldera (see Fig. 2 for location). For reference the atmospheric concentration of He and CH_4 are represented as horizontal lines. Note that the scale for CO_2 flux has been truncated to show details at the lower range; as such six samples having flux values between 1000 and 3000 g m^{-2} d^{-1} have been removed in the interval from 330 to 340 m.

recognisable (Fig. 8a). It is characterised by a main slip plane that is polished and striated, and which sometimes has associated abrasive slickensides. The striations and orientations of the slickensides, where present, are consistent with a predominantly normal slip, with minor left- or right-lateral slip components depending on the local orientations of the surfaces. In this case the fault core (sensu Caine et al., 1996; Chester et al., 1993) is very thin and poorly developed, a few millimetres thick, and composed of fine-grained material. The deformed rocks around the fault plane, i.e. the damage zone, consist of a 50–100 cm wide fracture zone. Fracture density around the fault plane is usually distributed asymmetrically, increasing towards the fault plane in the hanging wall compared to a relatively undeformed footwall. Deformation appears to be controlled exclusively by brittle processes and no evidence of fluid circulation on the slip plane or in the damage zone is recognisable.

The second style is referred to as ''fault network'' deformation, and it consists of an assemblage of normal faults and conjugate shear fracture systems having approximately the same strike (Fig. 8b). Fault plane kinematic indicators are mostly dip slip, and planes are generally at high angles to sigma 1. The fault network domains are 4–5 m wide and repeat every 8–10 m along the quarry face. Inside each domain the cross-cutting relationships among the fractures and striated slip surfaces are not univocal, suggesting that all of these structures belong to the same deformation event. Such synthetic and antithetic faults and fractures form a mesh (sensu Sibson, 1996, 2000) where interconnecting planes provide a conduit structure for fluid circulation. Although the preferred orientation for fluid circulation in meshes is parallel to the intersection of faults and fractures, as suggested by Sibson (1996), in this area fluid migrates to the surface from bottom to top. This is shown by the precipitation of sulphur crystals on the fault plane due to the upward migration of sulphur-rich fluids (hatched areas, Fig. 8b). Locally, where the network is not well developed and fractures are not completely interconnected, traces of sulphur crystals are observed on horizontal planes (parallel to fractures intersection) until a new vertical conduit is intersected.

The third deformation style is found in the central part of the quarry face, where a fault and its associated structures crops out (Fig. 9). This fault zone is almost symmetric and consists of two main slip planes which isolate the 5 m wide fault core from the surrounding 5–6 m wide damage zones. The two walls of the core are quite regular, planar-slip surfaces that are approximately parallel, sub-vertical, dip towards 150°, and have abrasive slickensides that indicate a normal sense of shear. The core zone comprises materials which vary in grain size with an almost symmetric distribution, consisting of mainly grey, clayey material mixed with small lithic fragments (about 10–20 mm in diameter), as well as clays, white pumice, and other black volcanic rocks. In the central part, up to 1 m diameter blocks of the host rock are encompassed in the clayey material, as are blocks of clays and other black lavas. The following sequence can be recognised from one slip plane to the other: 2 m of fine material, 1.5 m of breccias (including blocks of the host rock), and again about 1 m of fine material.

On both sides of the core the clayey material is non-cohesive. Here lithic fragments are observed as aligned bands of different grain sizes that dip towards 300°, showing a trend that is parallel to the fault wall. Close to the slip planes these bands exhibit a drag geometry that is compatible with the kinematics observed on the slip planes themselves. Small, smooth, and poorly developed slip surfaces present inside this zone cross-cut each other (Fig. 9b) and cut the mentioned lithic bands. These slip surfaces have the same attitude as the main slip planes, show abrasive kinematic indicators with normal, dip–slip movement, and could represent zones of higher cohesion and localised

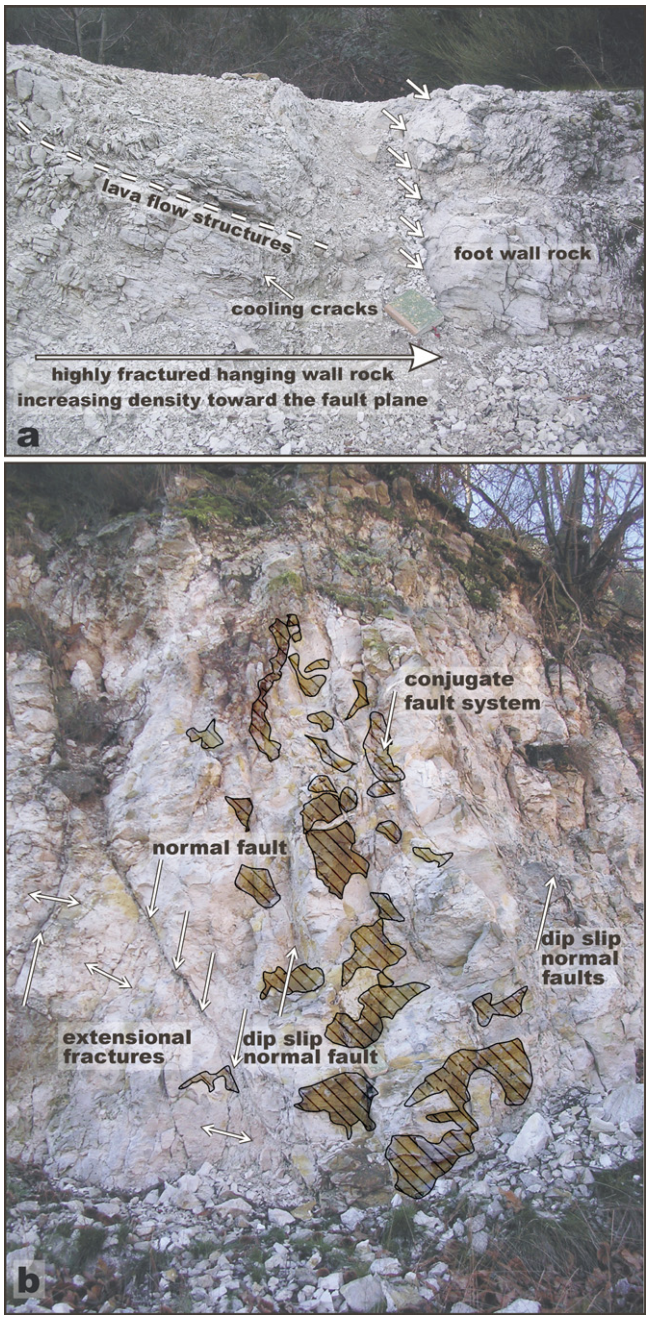

Fig. 8 – (a) Photo of a single fault plane, illustrating the occurrence of the main, polished and striated slip plane (series of arrows) and associated hanging wall deformation; (b) photo of a fault network, with the structural assemblage composed of normal faults and a shear fracture conjugate system. The hatch pattern highlights fault and fracture surfaces that are encrusted with sulphur precipitates.

shear stress; these features do not form a network inside the core zone. In general, fracture density in the clayey material is very low, and planes are often filled by reddish to black material that may also be related to surface water infiltration. In the central part, greater fracturing observed in host rock blocks does not continue into the clayey material.

Fracturing in the damage zone around the fault core is pervasive, and planes are clearly connected to each other as described for the fault network domain above (Figs. 8 and 9). This interval consists of a conjugate system of high-angle fractures and normal faults parallel to the main slip planes. These parts of the fault represent the main fluid conduit, as shown by the precipitation of sulphur minerals on the planes.

The large contrast between the lithic, cohesive host rock and the clayey material in the core might be explained not only by mechanical re-working and geochemical reactions induced by water and gas movement, but also by the simple filling of a soft, fault-core depression with fine-grained material. However, both the clayey material and the damage zones are deformed, and so even if some of the core material was originally deposited in this interval the final composition and structural configuration is to be attributed to mechanical and geochemical processes. Mineralogical and geochemical analyses of this composite material are in progress to better define these processes.

5.2.2. CO_2 flux

In total, 267 CO_2 flux measurements were collected along a regular grid on the quarry floor in front of the structures described above, with the results summarised in Table 1. The mean CO_2 flux value (1700 g m^{-2} d^{-1}) is very high due to the maximum value of 49563 g m^{-2} d^{-1}, while the median (331 g m^{-2} d^{-1}) is also very high because almost the entire gridded area of the quarry floor has anomalous flux rates. Data analysis with normal probability plots shows that a total of five different populations can be defined, each of which is linked to a particular migration environment. Only about 10% of the samples are in the background population (defined as 0–60 g m^{-2} d^{-1}), whereas all others can be considered as anomalous.

The extreme spatial variability of the site is highlighted by flux rate values that change by 2 orders of magnitude between sampling points separated by 3 m, while a separate test showed a change of more than 1 order of magnitude over only 30 cm. This clearly illustrates the ''spot'' nature of gas migration along spatially restricted channels (or ''pipes'') along the fault plane.

Directional experimental variograms conducted on the log-transformed CO_2 flux data highlight an anisotropy having a N50°E maximum axis. The computed experimental variograms were modelled along the maximum anisotropy axis, yielding the following equation: $\gamma = 0.32 + 0.2$ Sph (42 m) and an anisotropy ratio of 2. These results were used as parameters for the kriging calculations, which produced the CO_2 flux contour map given in Fig. 10. This map clearly illustrates a N50°E trend, while the shape of the anomalies confirms the highly anisotropic behaviour.

6. Discussion

6.1. *The structural control of gas migration*

The structural work performed throughout the Latera caldera area has defined normal kinematics along two principle

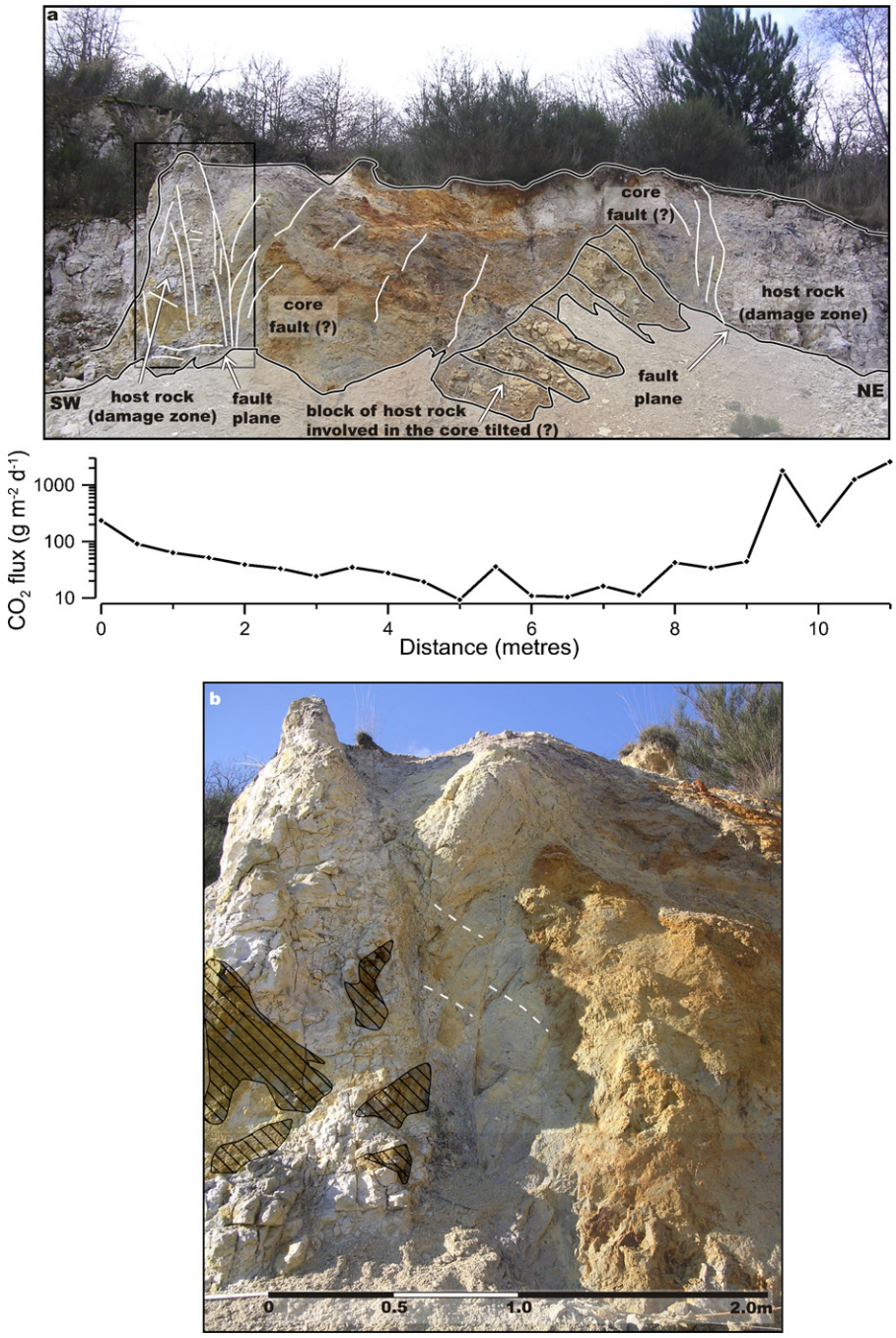

Fig. 9 – Mature fault in the site 3 quarry and the distribution of CO_2 flux across it (a). Note the symmetry of the fault with two damage zones and a central part consisting of clayey material. The two main faults, the blocks of the host rocks involved inside the core zone, and the deformation close to the wall faults are highlighted. (b) Detail of one of the faults outlined in (a), showing the bands inside the clayey material and their drag geometry close to the slip planes as well as the small and poorly developed slip surfaces. The fault/fracture surfaces stained by sulphur are outlined.

trends, one at N10°E and the other at N50°E (Fig. 4), which agree with the regional trends observed throughout northern Latium and in deep boreholes drilled in the caldera area itself for geothermal exploration (Sabatelli and Mannari, 1995). At the surface these features tend to be open in the brittle volcanic units in which they are found, providing a highly permeable pathway for CO_2 in the geothermal reservoir to escape towards the atmosphere.

This is clearly illustrated by the fact that the regional soil gas results (Fig. 6) also show preferential alignment between N–S and N50°E. In this figure, the values that are greater than the 2.5% contour can be considered as anomalous, based on an analysis of the normal probability plot for this dataset. Values below this threshold concentration are likely due to soil biological processes such as microbial and root respiration (e.g. Risk et al., 2002).

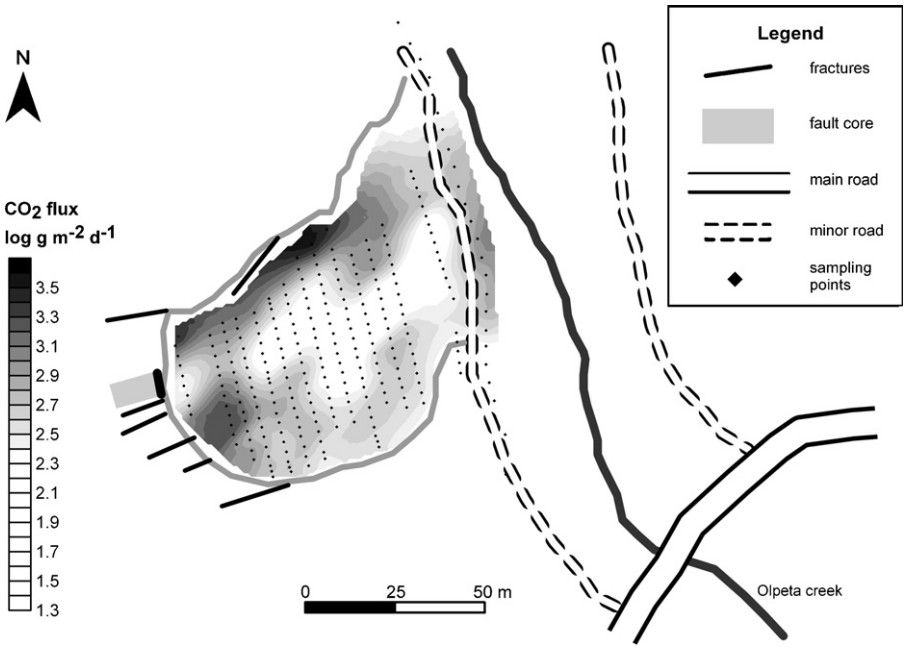

Fig. 10 – The contoured distribution of CO_2 flux in the site 3 quarry. Note the mapped orientation of fractures on the SW face of the quarry, including the interval of the "mature fault" shown by the grey box. Black dots show the sampling locations.

Although this figure, together with the geostatistical analysis, shows lineament directions that are similar to those of the measured faults and fracture systems, leakage does not occur along the entire length of any given fault but is instead focused at isolated points or small areas known as gas vents. This implies a complex permeability distribution along the fault planes, whereby gas flow occurs via preferential pathways consisting of well-interconnected, larger voids (i.e. gas is the non-wetting phase). The existence and location of these pathways, and the eventual gas release points on the surface, is controlled by a number of processes. At the pore scale these would include permeability reduction via secondary mineral precipitation (Cavarretta et al., 1985) or clay infilling (this study). At a larger scale, issues related to fault intersection and fault development can influence the distribution and nature of secondary permeability, as discussed below.

Fault intersection can result from one fault cross-cutting an older, unrelated fault that has a different orientation, or via the contact between a main fault and its related transfer structure. In either case this juncture could have increased dilation or brecciation, creating a more permeable, vertical, gas migration pathway above which soil gas anomalies may form (e.g. Fountain and Jacobi, 2000). The fault and fracture orientations measured in the Latera caldera cluster around the two directions of N10°E and N50°E, indicating the potential for intersecting structures. In addition, cross-cutting conjugate fracture patterns are observed in outcrop, and small-scale vertical offset is locally transferred from one main fault to another via high angle, normal/strike-slip faults. Based on observations of rock exposures, the N50°E fractures and faults appear to be relay ramps associated with the main fault system at N10°E. This seems to be in agreement with the variogram analysis of the regional soil gas CO_2 data, where the small-scale main anisotropy axis trends N45°E and the large-scale main anisotropy axis trends N20°E.

If gas migration pathways occur along the intersection of two faults, one might expect them to be more "pipe-like" (along the intersection) and to release gas at the surface from more spatially isolated spots. One gas vent that may meet these criteria is the so-called "gas vent A" (GVA), which has been studied extensively in Beaubien et al. (2008) and which occurs between 300 and 350 m in the profile shown in Fig. 7. This vent is clearly isolated, with a small (<10 m) core of high CO_2 flux rates (1000–3000 g m^{-2} d^{-1}) surrounded by a transition zone in which flux values return rapidly to background levels. A detailed soil gas grid conducted above this vent (data not shown) shows two anomaly orientations, implying that they may have formed at the juncture of two structures.

Fault development, along strike or in time, can also greatly influence secondary permeability due to changes in fracture interconnectivity and self-sealing processes. Such variations can be seen in the site 3 quarry, where the three-dimensional exposure allows for a better understanding of structure distribution and its influence on gas migration pathways. As described, three different deformation styles are observed here: style 1—simple, spatially restricted, single fault planes; style 2—more complex fault networks, where fractures are more developed, inter-connected, and secondary permeability is high; and style 3—mature faults, where the system has evolved a clay-rich fault core that is relatively impermeable.

Highly detailed gas flux measurements on the quarry floor show a distribution that agrees well with the structural observations made on the quarry walls (Fig. 4). In the middle of the quarry floor an interval of low CO_2 flux extends from the central, clay-rich mature fault core (i.e. style 3) in a direction

that is essentially the same as the measured fracture patterns. On the northern edge of this low-flux interval there is an alignment (N50°E) of extremely high values (up to 40,000 g m^{-2} d^{-1}) that lie along strike with the damage zone of the main fault (which is similar to the style 2 deformation); along the quarry face this interval shows highly brittle deformation with large cavities and open, interconnected fractures. Finally, some isolated anomalies appear to correspond with style 1 deformation, however these tend to be less continuous and less pronounced.

The effect of these different styles can be seen schematically in Fig. 11. Here the distribution of CO_2 soil gas or flux above a fault is shown to be controlled by the state of fault evolution (e.g. styles 2 or 3). If style 2 dominates there will be a well-developed fracture network on which gas migration will tend to be centred (Fig. 11a). Where such a feature is buried beneath shallow sediments, a distribution may occur like that observed from 400 to 500 m along the site 5 profile (Fig. 7). Here the anomaly is wide, irregular, and values are generally much lower than those observed in isolated GVA, implying a wide fracture network where gas flux maximums are reduced due to the division of flow into a larger number of escape pathways.

Instead, if the feature is a mature fault with a well developed cataclastic/gouge core bounded by a highly fractured damage zone (i.e. style 3), values above the low-permeability fault core would be low and two peaks would occur above the lateral fracture zones (Fig. 11b), as is seen in the site 3 quarry (Figs. 9a and 10). Such a double peak distribution has also been observed in profiles conducted across the San Andreas Fault in California, with a similar fault architecture being proposed as the controlling mechanism (King et al., 1996). Although recent research has shown that these observed anomalies may not be due to deep gas migration, but rather to wind-induced movement of biogenic and near-surface gases within the bounding fracture zones (Lewicki and Brantley, 2000; Lewicki et al., 2003), the structural architecture still remains valid.

It should be remembered that the three styles observed at site 3 may represent not only an evolution in time as the fault matures, but also in space due to differential movements or the intersection of different lithologies (e.g. Baubron et al., 2002). In terms of spatial distribution, this along-strike change in permeability would have a fundamental impact on the nature of surface CO_2 release, with gas flux or soil gas anomalies being perhaps aligned but not continuous, or parallel but not aligned (e.g. Ciotoli et al., 2007). In between these anomalies there may be no gas flow, although individual "spot anomalies" may begin to coalesce if they are sufficiently close to each other (e.g. Lewicki et al., 2007c). An example of a no-flow regime is shown by the long interval of background soil gas concentrations ($CO_2 < 2.5\%$, $He < 5.25$ ppm; $CH_4 < 1.5$ ppm) and CO_2 flux values (<22 g m^{-2} d^{-1}) observed from 50 to 200 m in Fig. 7, indicating that there are large blocks of intact volcanics (and overlying sediments) that impede deep CO_2 migration.

Thus the results given in Fig. 7 indicate that gas release at surface is primarily controlled by faults, and argue against large-scale diffuse degassing (sensu Chiodini et al., 2007) in this area (although more research is needed to better understand if it is occurring elsewhere). Instead, the size of an anomaly appears to be controlled by lateral migration and chemical/biological processes occurring in the vadose zone, as discussed below.

6.2. *Gas migration through the vadose zone*

Conceptually, gas ascending from the geothermal reservoir at Latera will migrate as bubble or continuous gas flow along

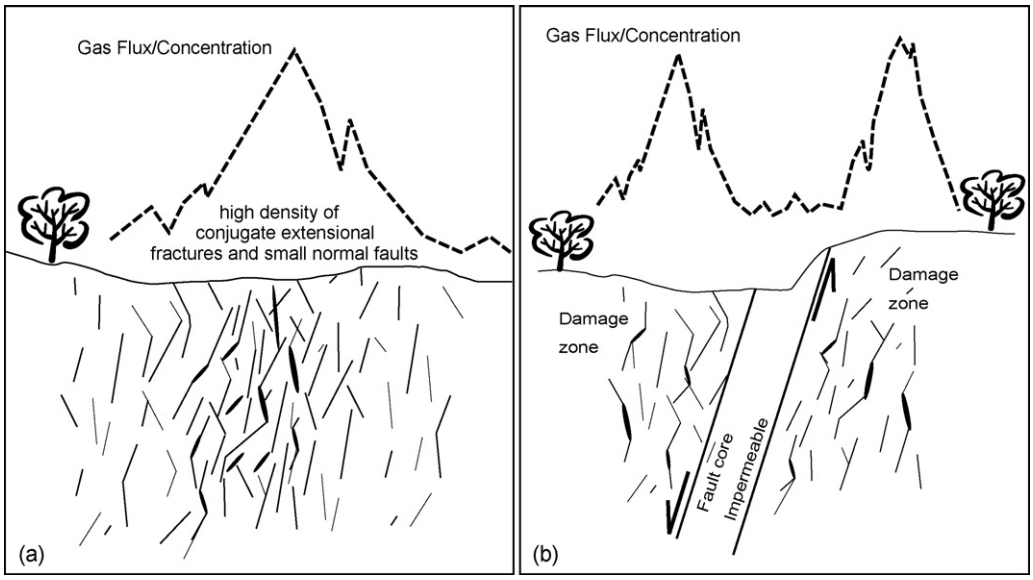

Fig. 11 – Schematic drawing showing different structural assemblages and their influence on CO_2 leakage; these stages of deformation could represent changes either in time as the fault develops, or along strike due to differential movements. (a) The fault network configuration results in more open, interconnected gas migration pathways, resulting in higher gas flux rates. (b) The mature fault shows the development of a very low permeability core, bounded by damage zones that maintain the fault network character.

faults and fracture systems until the water table is encountered, after which migration will occur via gas-phase advective or diffusive flow in the unsaturated vadose zone. Gas will also dissolve into the groundwater and then be transported laterally via groundwater flow, however this mechanism is not addressed here. The vadose zone can either consist of bedrock, such as that observed in the site 3 quarry, or of shallow sediments and soil, as occurs at site 5. Depending on the thickness, porosity and permeability, water content, microbiology, and chemistry of the unsaturated zone, the deep-gas signature originating from the fault will be altered to some degree. Such a change will influence our ability to locate CO_2 leakage (especially from buried faults) with any near-surface monitoring technique, such as gas-geochemistry, atmospheric, biological, or remote-sensing measurements. The following discusses the influence of the vadose zone at the Latera site.

The distribution of anomalous soil gas CO_2 is wider than the intervals of highest CO_2 flux, as illustrated by a detailed portion of the site 5 profile (Fig. 12). The wide interval of anomalous soil gas CO_2 (from about 300 to 370 m), as compared to the core of very elevated CO_2 flux values (from 328 to 342 m), is likely linked to the horizontal migration of soil gas CO_2 via both advective forces and density-driven flow. For example a numerical modelling study conducted by Altevogt and Celia (2004) found that vertical and horizontal pressure gradients become similar at higher flow rates and that the density contrast between air and CO_2 can result in more lateral

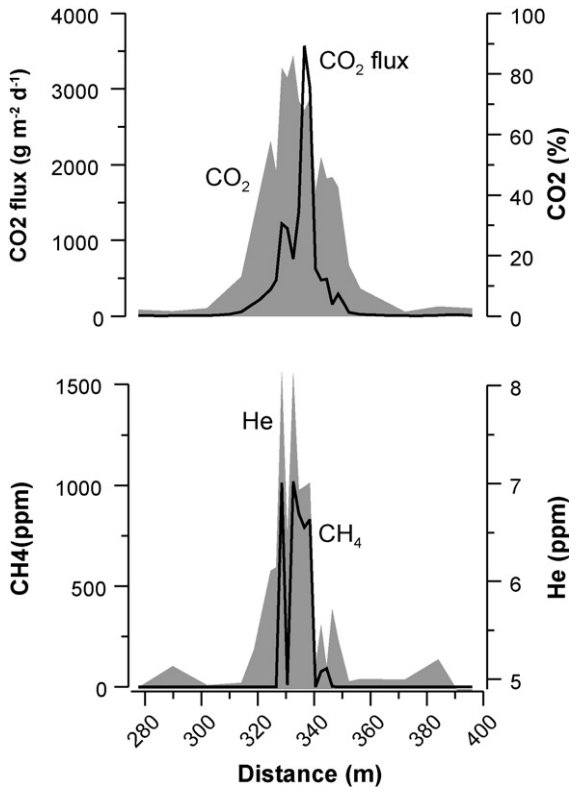

Fig. 12 – Detail of the site 5 profile. Compared to the complete profile given in Fig. 7, this figure shows the CH_4 data plotted on a normal scale and the CO_2 flux data are not truncated.

spreading and storage of CO_2 in the unsaturated zone. Similar lateral distributions in the vadose zone were also found by Lewicki et al. (2007c) in simulations of a CO_2 release slightly below the water table. The observed distribution of CO_2 may also be slightly attenuated from even-further lateral migration due to mass loss via dissolution into pore water and subsequent involvement in acidic reactions with the sediments (Altevogt and Jaffe, 2005).

Other proposed mechanisms for increased soil gas CO_2 values peripheral to a vent include the return of released CO_2 via dissolution in falling rainwater or back diffusion from the atmosphere (Oldenburg and Unger, 2004). As sampling was conducted during the dry season, infiltration need not be considered here, whereas the steady increase in CO_2 concentrations with depth in vertical profiles conducted around the vent (not shown) argues against a major contribution from back diffusion from the atmosphere.

Fig. 12 shows the distribution of anomalous He values to be narrower than that of CO_2, but in good correspondence with the interval of moderately elevated CO_2 flux values (i.e. from 312 to 355 m). The slightly lower lateral migration of He, compared to CO_2, may be the result of such factors as: (i) helium has a lower density than air, and thus density-driven flow is not an issue but instead buoyancy forces may result in an additional vertical flow component; (ii) helium is much less soluble than CO_2, and thus there is no potential for storage in pore water and subsequent equilibrium exchange with the gas phase; and (iii) the ratio between deep gas and background soil air concentration is much lower for He (<2) than for CO_2 (about 100) at this site, and thus He diffusion gradients will be lower (thereby minimising the effect of the higher He diffusion coefficient). It should also be remembered that He is non-reactive, and thus no chemical attenuation mechanism exists like that described above for CO_2. Such considerations may also be important for the use of other tracer gases that have been proposed to monitor for leakage from CO_2 geological storage sites, such as sulphurhexafluoride (SF_6) or various perfluorocarbon gases (e.g. Wells et al., 2007), as their physical–chemical characteristics are similar to those of He (i.e. non-reactive, highly mobile, etc.). That said, artificial tracers have the advantage of very low natural concentrations, thus detection limits are very low and there is the potential for large concentration gradients that may promote lateral diffusion.

The distribution of anomalous CH_4 concentrations is even more restricted than that of He, as shown by the limited number of samples along the site 5 profile (Fig. 7) with values above that of atmospheric air (1.8 ppm): at 425 m (4.4 ppm) and in gas vent A from 325 to 345 m (up to 1000 ppm). The CH_4 results for GVA are more clearly seen in Fig. 12, where they are plotted on a normal scale. Here one can see that anomalous CH_4 values exist at 80 cm depth only in the interval where CO_2 flux values are at their maximum (from 328 to 342 m). In contrast to both CO_2 and He, CH_4 is redox reactive and readily oxidised in aerobic soils (e.g. Castaldi et al., 2007), meaning that CH_4 concentrations in well-aerated soils are typically below atmospheric concentrations. As discussed in more detail by Beaubien et al. (2008), this reactive gas (and others such as hydrogen sulphide, hydrogen, and ethane) is maintained in the anoxic core of the vent, but is rapidly oxidised as

it migrates laterally into zones with higher O_2 concentrations. Considering its distribution in Figs. 7 and 12, it appears that a CO_2 flux rate greater than 500 g m^{-2} d^{-1} is needed to create an environment, in these soils and at this depth, in which CH_4 remains stable.

Although the analysis of as many gas species as possible will improve the potential for identifying and locating a leak above a geological CO_2 storage site, the effectiveness of an individual gas species may be influenced by its spatial distribution and the size of anomaly that it may produce (as described above). In addition, any monitoring program above a CO_2 geological storage site must try to enhance the potential for success while at the same time keeping costs acceptable. To balance these two issues of success rate and costs, and considering the observation that CO_2 has the largest ''footprint'' around a leak while other gas species are more spatially restricted (but potentially more indicative of a deep origin), one could consider the following approach: a large number of points could be measured in the field for CO_2 flux and soil gas CO_2, and then at locations where field results are above a pre-set threshold a soil gas sample could also be collected for the laboratory analysis of other species (and/or isotopes). As an experienced technician can do field measurements at 30–70 points per day (depending on terrain and sample spacing) there is the potential to measure a large number of sites with this approach, which will allow for a higher sample density and a greater potential for locating what may be a spatially small anomaly. Subsequently, the laboratory analysis of various tracer gases (He, CH_4, artificial tracers, isotopes, etc.) on only those samples having anomalous CO_2 flux or concentration will then help define the origin of the anomaly (deep or shallow) while at the same time keeping costs low. Subsequent detailed sampling grids or profiles could also be measured around an anomaly to help confirm its origin and to define its lateral extent. The types of gases used for separating deep – from shallow – origin CO_2 anomalies should be chosen based on the type of storage reservoir being studied. For example, CH_4 and He would be good choices for monitoring above a CO_2-EOR site because they are naturally associated with the reservoir, whereas artificial tracers added to the CO_2 injection stream might be preferred above a deep saline aquifer.

It must be stressed, however, that this approach is based on the results obtained from an essentially steady-state system having site-specific conditions (e.g. vadose zone thickness, sediment permeability and composition, climate and rainfall, gas flow rate and composition, etc.); it is recommended that similar work be conducted on other sites with different settings to extend the results obtained here.

7. Conclusions

Structural geology and near-surface gas geochemistry surveys conducted within the Latera caldera, where naturally produced CO_2 is leaking to the atmosphere, have highlighted a number of issues related to the migration of gas along faults and its eventual transfer to the atmosphere.

Both detailed and regional soil gas and gas flux measurements have the same general trends as those measured in outcrops and in deep boreholes (approximately N10°E and N45°E), showing that migration is controlled by these structures. Release at surface, however, is not continuous along strike, but instead occurs at determined places due to channelled flow along more permeable pathways along the fault plane. Work on an exposed fault shows a clear link between deformation style, secondary permeability characteristics, and the spatial distribution and mass transfer rates of deep gas to the surface. These styles represent not only temporal changes in a fault system during its evolution, but may also be the result of spatial changes caused by differential movements or the intersection of different lithologies along strike; this variability clearly has an influence on the distribution of gas migration at surface. For example a detailed gas geochemistry profile conducted across buried faults showed different types of venting features, ranging from isolated, high-flux-rate gas vents that may have formed at the juncture of two faults (concentrated ''pipe'' flow) to wider areas of more diffuse degassing which may be related to a wide damage zone of networked fractures (diffuse ''sheet'' flow). Wide intervals occur between these degassing sites where all measured parameters are at background values, indicating that there are unfaulted blocks of volcanic rocks and overlying sediments that represent barriers to upward gas migration.

Movement of the deep gases in the vadose zone was also examined, particularly with detailed sampling across an isolated gas vent (GVA). These results show how the CO_2 flux rate and distribution is important for controlling the subsurface distribution of the various migrating gases, but that the individual chemical–physical characteristics of each gas results in different behaviours. Soil gas CO_2 at 80 cm depth was found to have the widest lateral distribution (mirrored by opposite O_2 and N_2 trends), He was narrower, while reactive gas species like CH_4 and H_2S were very narrow and restricted to the highest CO_2 flux interval in the vent core. Different diffusion coefficients, redox reactivity, gas density, and concentration gradients are believed to be some of the more important controlling parameters.

The results of this study have many implications for CO_2 geological storage. To begin with the necessity of a thorough knowledge and understanding of the structural geology of any site considered for geological CO_2 storage has been highlighted through the close link found between faults and gas migration in the Latera caldera. Such site characterisation, which would help to focus future monitoring on areas which might have a higher risk, could also include near-surface gas geochemistry techniques to search for any gas-permeable structures. As seen here regional surveys have the potential to outline anomalies, depending on the sampling density and size of any eventual leak. However any results must be subsequently checked using detailed sampling grids or horizontal profiles. In addition, the distribution of leaking deep gases in the soil has been shown to depend both on vadose zone characteristics and the physical–chemical properties of each gas species, and that this information should be considered in the design of any near-surface gas geochemistry monitoring program.

This research has shown how the study of natural systems like that at Latera permits us to better understand gas migration relative to the issues of scale, heterogeneity, and system evolution, thus improving our ability to choose, construct, and monitor safe CO_2 geological storage sites. Even if a volcanic terrain will likely never be chosen for a geological storage site, it

is believed that the issues raised in this article and many of the processes and mechanisms observed at Latera can be used in other geological settings.

Acknowledgements

We would like to thank Anna Baccani for her help during the laboratory analyses, Mr. Iacarelli for his kind access to one of the study sites, and Lucio Poscia of the local Latera administration for his support in the field and for giving access to the abandoned quarry at site 3. Some data presented here was collected within the European-Community funded project on natural analogues of CO_2 geological storage (NASCENT), while the rest was conducted within the European-Community funded Network of Excellence on CO_2 geological storage (CO2GeoNet). The authors would also like to sincerely thank two anonymous reviewers for their thoughtful comments and suggestions, which significantly improved the manuscript.

Appendix A. Geological setting of the Latera caldera

A.1. *Pre-volcanic sedimentary sequences*

There are five main sedimentary sequences that were deposited in the area prior to volcanic activity: (i) Triassic to Oligocene marine sediments of the Tuscan domain, consisting of Triassic to Lower Cretaceous limestones and marls (Tuscan sequence) and Cretaceous to Oligocene sandstones, turbiditic limestones and argillites (Tolfa Flysch); (ii) Triassic to Oligocene marine sediments of the Umbria domain, consisting of evaporites, limestones and marls; (iii) Lower Cretaceous to Paleocene allochthonous flysch of the Ligurid domain, consisting of marine shales, siltstones and marls with subordinate sandstones; (iv) Miocene continental sediments consisting of conglomerates and shales deposited prior to volcanic activity; and (v) Upper Pliocene–Upper Calabrian marine to brackish sediments, represented by clays and sandy-clays with polygenic conglomerates (Bertini et al., 1971). These sedimentary formations randomly crop out in the Vulsini Volcanic district, although they are more continuous near Mt. Razzano, where a NS-syncline deforms the Tuscan formations (Buonasorte et al., 1991), and Mt. Canino, where the Liassic to Cretaceous Tuscan sequence forms a NS-trending anticline and syncline. The same lithologies are crossed in deep geothermal exploration wells throughout the area.

A.2. *Volcanic sequences*

The Latera Volcanic complex developed in the western part of the Vulsini district between 0.3 and 0.1 Ma (Palladino and Simei, 2005; Simei et al., 2006; Vezzoli et al., 1987). Although the Latera caldera has a relatively simple topography, its eruptive history is complex (Fig. 3), with multiple depocentres and a close link to Quaternary extensional tectonics. The main steps of the caldera evolution are related to three main eruptions (Sovana, Onano and Pitigliano; Fig. 3) that occurred from 0.19 to 0.16 Ma ago (Palladino and Simei, 2005). The Latera caldera is the main edifice to the west of the Bolsena caldera, and it marks a change from previously dominant effusive volcanism (around 0.4–0.3 Ma) to explosive volcanism characterised by a wide spectrum of potassic rock types. This explosive nature resulted in a polygenic collapse caldera which has been dated at 0.3 Ma (Palladino and Agosta, 1997; Palladino and Simei, 2005; Palladino and Valentine, 1995; Sparks, 1975; Trigila and Walker, 1981; Vezzoli et al., 1987), followed by recurrent Plinian activity 0.28–0.23 Ma which formed a central volcanic edifice Palladino and Agosta, 1997; Palladino and Simei, 2005). The subsequent Sovana eruption resulted in pyroclastic flow activity (around 0.19 Ma) and is related to the main collapse of the Latera caldera. The largest volume of volcanic products was then erupted during the Onano eruption (0.17 Ma), which occurred from a fissure-like vent bordering the Latera caldera to the east instead of a central volcanic edifice (Freda et al., 1990; Nappi, 1969; Vezzoli et al., 1987). The final phases of activity were characterised by the migration of emission epicentre from east to the northwest, where the Pitigliano eruption took place at 0.16 Ma and generated the small Vepe caldera (Nappi et al., 1991). Subsequent activity was then limited to effusive and hydromagmatic eruptions from multiple monogenetic centres both within and outside of the Latera caldera (Palladino and Simei, 2005).

REFERENCES

Agosta, F., Aydin, A., 2006. Architecture and deformation mechanism of a basin-bounding normal fault in Mesozoic platform carbonates, central Italy. Journal of Structural Geology 28, 1445–1467.

Altevogt, A.S., Celia, M.A., 2004. Numerical modelling of carbon dioxide in unsaturated soils due to deep subsurface leakage. Water Resources Research 40 (W03509), doi:10.1029/2003WR002848.

Altevogt, A.S., Jaffe, P.R., 2005. Modelling the effects of gas phase CO_2 intrusion on the biogeochemistry of variably saturated soils. Water Resources Research 41 (W09426), doi:10.1029/2004WR003819.

Anderson, D.E., Farrar, C.D., 2001. Eddy covariance measurement of CO_2 flux to the atmosphere from an area of high volcanogenic emissions, Mammoth Mountain, California. Chemical Geology 177, 31–42.

Antonellini, M., Aydin, A., Pollard, D., 1994. Microstructure of deformation bands in porous sandstones at Arches National Park, Utah. Journal of Structural Geology 16, 941–959.

Azzaro, R., Branca, S., Giammanco, S., Gurrieri, S., Rasa, R., Valenza, M., 1998. New evidence for the form and extent of the Pernicana Fault System (Mt. Etna) from structural and soil-gas surveying. Journal of Volcanology and Geochemical Research 84, 143–152.

Baines, S.J., Worden, R.H., 2004. The long-term fate of CO_2 in the subsurface: natural analogues for CO_2 storage. In: Baines, S.J., Worden, R.H. (Eds.), Geological Storage of Carbon Dioxide, Special Publication, 233. The Geological Society of London, London, pp. 59–86.

Barberi, F., Innocenti, F., Landi, P., Rossi, U., Saitta, M., Santacroce, R., Villa, I.M., 1984. The evolution of Latera caldera (central Italy) in the light of subsurface data. Bulletin of Volcanology 47, 125–141.

Barton, C.A., Zoback, M.A., Moos, D., 1995. Fluid flow along potentially active faults in crystalline rock. Geology 23, 683–686.

Bateson, L., Vellico, M., Beaubien, S.E., Pearce, J.M., Ciotoli, G., Annunziatellis, A., Coren, F., Lombardi, S., Marsh, S., 2008. Preliminary results of the application of remote sensing techniques to detecting and monitoring leaks from CO_2 storage sites. International Journal of Greenhouse Gas Control 2 (3), 388–400.

Baubron, J.C., Rigo, A., Toutain, J.P., 2002. Soil gas profiles as a tool to characterise active tectonic areas: the Jaut Pass example (Pyrenees, France). Earth and Planetary Science Letters 196, 69–81.

Beaubien, S.E., Ciotoli, G., Coombs, P., Dictor, M.C., Krüger, M., Lombardi, S., Pearce, J.M., West, J.M., 2008. The impact of a naturally occurring CO_2 gas vent on the shallow ecosystem and soil chemistry of a Mediterranean pasture (Latera Italy). International Journal Greenhouse Gas Control 2 (3), 373–387.

Beaubien, S.E., Ciotoli, G., Lombardi, S., 2003. Carbon dioxide and radon gas hazard in the Alban Hills area (central Italy). Journal of Volcanology and Geothermal Research 123, 63–80.

Beaubien, S.E., Lombardi, S., Ciotoli, G., Annunziatellis, A., Hatziyannis, G., Metaxas, A., Pearce, J.M., 2005. Potential hazards of CO_2 leakage in storage systems—learning from natural systems. In: Rubin, E.S., Keith, D.W., Gilboy, C.F. (Eds.), Proceedings of the 7th International Conference on Greenhouse Gas Control Technologies, vol. 1. Peer-Reviewed Papers and Plenary Presentations. Elsevier, Oxford, UK, pp. 551–560.

Bergfeld, D., Evans, W.C., Howle, J.F., Farrar, C.D., 2006. Carbon dioxide emissions from vegetation-kill zones around the resurgent dome of Long Valley caldera, eastern California, USA. Journal of Volcanology and Geothermal Research 152, 140–156, doi:10.1016/j.jvolgeores.2005.11.003.

Bertini, G., D'Amico, C., Deriu, M., Tagliavini, S., Vernia, L., 1971. Note illustrative della Carta Geologica d'Italia alla scala 1:100.000. Foglio 143 Bracciano. Roma, Serv. Geol. d'Italia.

Bertrami, R., Cameli, G.H., Lovari, F., Rossi, U., 1984. Discovery of Latera geothermal field: problems of the exploration and research. In: Seminar on Utilization of Geothermal Energy for Electric Power Production and Space Heating, Florence, 14–17 May 1984.

Brennan, S.T., Hughes, A.V., Friedmann, S.J., Burruss, R.C., 2004. Natural gas reservoirs with high CO_2 concentrations as natural analogues for CO_2 storage. In: The 7th Greenhouse Gas Control Technologies Conference (GHGT7), Vancouver, Canada, 5–9 September 2004.

Bruhn, R.L., Parry, W.T., Yonkee, W.A., Thompson, T., 1994. Fracturing and hydrothermal alteration in normal fault zones. Pure and Applied Geophysics 142, 611–643.

Buonasorte, G., Ciccacci, S., De Rita, D., Fredi, P., Lupia Palmieri, E., 1991. Some relations between morphological characteristics and geological structure in the Vulsini Volcanic Complex (Northern Latium, Italy). Zeitschrift fuer Geomorphologie Supplement BD 82, 59–71.

Caine, J.S., Evans, J.P., Forster, C.B., 1996. Fault zone architecture and permeability structure. Geology 24, 1025–1028.

Caine, J.S., Forster, C.B., 1999. Fault zone architecture and fluid flow: insight from field data and numerical modeling. In: Haneberg, W.C., Mozley, P.S., Moore, J.C., Goodwin, L.B. (Eds.), Faults and Subsurface Fluid Flow, Geophysical Monograph 113. pp. 101–128.

Carmignani, L., Kligfield, R., 1990. Crustal extension in the Northern Apennines: the transition from compression to extension in the Alpi Apuane core complex. Tectonics 9, 340–349.

Castaldi, S., Costantini, M., Cenciarelli, P., Ciccioli, P., Valentini, R., 2007. The methane sink associated to soils of natural and agricultural ecosystems in Italy. Chemosphere 66, 723–729.

Cavarretta, G., Giannelli, G., Scandiffio, G., Tecce, F., 1985. Evolution of the Latera Geothermal System II: metamorphic, hydrothermal mineral assemblages and fluid chemistry. Journal of Volcanology and Geochemical Research 26, 337–364.

Chadwick, A., Arts, R., Eiken, O., Williamson, P., Williams, G., 2006. Geophysical monitoring of the CO_2 plume at Sleipner, North Sea. In: Lombardi, S., Altunina, L.K., Beaubien, S.E. (Eds.), Advances in the Geological Storage of Carbon Dioxide. NATO Science Series. IV. Earth and Environmental Sciences, vol. 65. Springer, Dordrecht, The Netherlands, pp. 303–314.

Chester, F.M., Evans, J.P., Biegel, R.L., 1993. Internal structure and weakening mechanisms of the San Andreas faults. Journal of Geophysical Research 98, 771–786.

Chester, F.M., Logan, J.M., 1986. Implications for mechanical properties of brittle faults from observations of the Punchbowl fault zone, California. Pure Applied Geophysics 124, 79–106.

Chiodini, G., Baldini, A., Barberi, F., Carapezza, M.L., Cardellini, C., Frondini, F., Granieri, D., Ranaldi, M., 2007. Carbon dioxide degassing at Latera caldera (Italy): evidence of geothermal reservoir and evaluation of its potential energy. Journal of Geophysical Research 112 (B12204), doi:10.1029/2006JB004896.

Chiodini, G., Frondini, F., 2001. Carbon dioxide degassing from the Albani Hills volcanic region, central Italy. Chemical Geology 177, 67–83.

Chiodini, G., Frondini, F., Ponziani, F., 1995. Deep structures and carbon dioxide degassing in central Italy. Geothermics 24, 81–94.

Ciotoli, G., Lombardi, S., Annunziatellis, A., 2007. Geostatistical analysis of soil gas data in a high seismic intermontane basin: the Fucino Plain, central Italy. Journal of Geophysical Research 112 (B05407), doi:10.1029/2005JB004044.

Cowie, P.A., Scholz, C.H., 1992. Growth of faults by accumulation of seismic slip. Journal of Geophysical Research 97, 11085–11095.

Di Filippo, M., Lombardi, S., Nappi, G., Reimer, G.M., Renzulli, A., Toro, B., 1999. Volcano tectonic structures, gravity and helium in geothermal areas of Tuscany and Latium (Vulsini volcanic district), Italy. Geothermics 28, 377–393.

Duchi, V., Minissale, A., Paolieri, M., Prati, F., Valori, A., 1992. Chemical relationship between discharging fluids in the Siena-Radiocfani Graben and the deep fluids produced by the geothermal fields of Mt. Amiata, Torre Alfina and Latera. Geothermics 21 (3), 401–413.

Evans, J.P., Foster, C.B., Goddard, J.V., 1997. Permeability of fault-related rocks, and applications for hydraulic structure of fault zones. Journal of Structural Geology 19, 1393–1404.

Evemden, J.F., Curtis, G.H., 1965. K/Ar of late Cenozoic rocks in Eastern Africa and Italy. Current Anthropology 6, 343–385.

Flodin, E.A., Gerdes, M., Aydin, A., Wiggins, W.D., 2005. Petrophysical properties of cataclastic fault rock in sandstone. In: Sorkhabi, R., Tsuji, Y. (Eds.), Faults, Fluid Flow, and Petroleum Traps. AAPG Memoir, vol. 85. pp. 197–227.

Fountain, J.C., Jacobi, R.D., 2000. Detection of buried faults and fractures using soil gas analysis. Environmental and Engineering Geoscience 6 (3), 201–208.

Freda, C., Palladino, D.M., Pignatti, S., Trigila, R., Onorati, G., Poscolieri, M., 1990. Volcano-tectonic scenario of Vulsini Volcanoes (Central Italy) from LANDSAT-MSS images and digital elevation data. Journal of Photogrammetry and Remote Sensing 45, 316–328.

Funiciello, R., Parotto, M., 1978. Il substrato sedimentario nell'area dei Colli Albani: considerazioni geodinamiche e

paleogeografiche sul margine tirrenico dell'Appennino Centrale. Geologica Romana 17, 233–287.
Gambardella, B., Cardellini, C., Chiodini, G., Frondini, F., Marini, L., Ottonello, G., Vetushi Zuccolini, M., 2004. Fluxes of deep CO_2 in the volcanic areas of central-southern Italy. Journal of Volcanology and Geothermal Research 136, 31–52.
Gaus, I., Le Guern, C., Pearce, J.M., Pauwels, H., Shepherd, T.J., Hatziyannis, G., Metaxas, A., 2004. Comparison of long-term geochemical interactions at two natural CO_2-analogues: Montmiral (Southeast Basin, France) and Messokampos (Florina Basin, Greece) case studies.In: The 7th Greenhouse Gas Control Technologies Conference (GHGT7), Vancouver, Canada, 5–9 September 2004.
Gerlach, T.M., Doukas, M.P., McGee, K.A., Kessler, R., 2001. Soil efflux and total emission rates of magmatic CO_2 at the Horseshoe Lake tree kill, Mamoth Mountain, California, 1995–1999. Chemical Geology 177, 101–116.
Gianelli, G., Scandiffio, G., 1989. The Latera geothermal system (Italy): chemical composition of the geothermal fluid and hypotheses on its origin. Geothermics 18, 447–463.
Gibson, R.G., 1994. Fault zone seals in siliciclastic strata of the Columbia basin, offshore Trinidad. American Association of Petroleum Geologists Bulletin 78, 1373–1385.
Gray, M.B., Stamatakos, J.A., Ferrill, D.A., Evans, M.A., 2005. Fault-zone deformation in welded tuffs at Yucca Mountain, Nevada, USA. Journal of Structural Geology 27, 1873–1891.
Haynekamp, M.R., Goodwin, L.B., Mozley, P.S., Haneberg, W.C., 1999. Controls on fault zone architecture in poorly lithified sediments, Rio Grande rift, New Mexico: implications for fault-zone permeability and fluid flow. In: Haneberg, W.C., Mozley, P.S., Moore, J.C., Goodwin, L.B. (Eds.), Faults and Subsurface Fluid Flow. Geophysical Monograph 113. pp. 27–50.
Hinkle, M., 1994. Environmental conditions affecting concentrations of He, CO_2, O_2 and N_2 in soil gases. Applied Geochemistry 9, 53–63.
Holloway, S., Pearce, J.M., Hards, V.L., Ohsumi, T., Gale, J., 2007. Natural emissions of CO_2 from the geosphere and their bearing on the geological storage of carbon dioxide. Energy 32, 1194–1201.
Hutchinson, G.L., Livingston, G.P., 1993. Use of chamber systems to measure trace gas fluxes. Agricultural ecosystem effects on trace gases and global climate change. ASA Special Publication, no. 55.
Hutchinson, G.L., Mosier, A.R., 1981. Improved soil cover method for field measurement of nitrous oxide fluxes. Soil Science Society of America Journal 45, 311–316.
IPCC, 2005. IPCC Special Report on Carbon Dioxide Capture and Storage. Prepared by Working Group III of the Intergovernmental Panel on Climate Change. In: Metz, B., Davidson, O., de Coninck, H.C., Loos, M., Meyer, L.A. (Eds.), Cambridge University Press, Cambridge, United Kingdom, New York, NY, USA, p. 442.
IPCC, 2007. Climate change 2007: the physical science basis. Contribution of Working Group I to the Fourth Assessment Report of the Intergovernmental Panel on Climate Change. In: Solomon, S., et al. (Eds.), Cambridge University Press, Cambridge, United Kingdom/ New York, NY, USA, p. 996.
King, C.Y., King, B.S., Evans, W.C., Zang, W., 1996. Spatial radon anomalies on active faults in California. Applied Geochemistry 11, 497–510.
Le Nindre, Y.M., Pauwels, H., Rubert, Y., Shepherd, T.J., Pearce, J.M., 2006. CO_2 trapping at geological time scale: geohistory of a natural analogue for long-term storage. In: The 8th Greenhouse Gas Control Technologies Conference (GHGT8), Trondheim, Norway, 19–22 June 2006.
Lewicki, J.L., Birkholzer, J., Tsang, C.F., 2007a. Natural and industrial analogues for leakage of CO_2 from storage reservoirs: identification of features, events, and processes and lessons learned. Environment Geology 52, 457–467, doi:10.1007/s00254-006-0479-7.
Lewicki, J.L., Brantley, S.L., 2000. CO_2 degassing along the San Andreas fault, Parkfield, California. Geophysical Research Letters 27 (1), 5–8.
Lewicki, J.L., Evans, W.C., Hilley, G.E., Sorey, M.L., Rogie, J., Brantley, S.L., 2003. Shallow soil CO_2 flow along the San Andreas and Calaveras Faults, California. Journal of Geophysical Research 108 (B4), 2187, doi:10.1029/2002JB002141.
Lewicki, J.L., Hilley, G.E., Tosha, T., Aoyagi, R., Yamamoto, K., Benson, S.M., 2007b. Dynamic coupling of volcanic CO_2 flow and wind at the Horseshoe Lake tree kill, Mammoth Mountain, California. Geophysical Research Letters 34 (L03401), doi:10.1029/2006GL028848.
Lewicki, J.L., Oldenburg, C.M., Dobeck, L., Spangler, L., 2007c. Surface CO_2 leakage during two shallow subsurface CO_2 releases. Geophysical Research Letters 34 (L24402), doi:10.1029/2007GL032047.
Lombardi, G., Mattias, P., 1987. The kaolin deposits of Italy. L'Industria Mineraria 6, 1–34.
Lombardi, S., Annunziatellis, A., Beaubien, S.E., Ciotoli, G., Coltella, M., 2008. Natural analogues and test sites for CO_2 geological sequestration: experience at Latera, Italy. First Break 26, 39–43.
Lombardi, S., Annunziatellis, A., Ciotoli, G., Beaubien, S.E., 2006. Near surface gas geochemistry techniques to assess and monitor CO_2 geological sequestration sites. In: Lombardi, S., Altunina, L.K., Beaubien, S.E. (Eds.), Advances in the Geological Storage of Carbon Dioxide. NATO Science Series, IV. Earth and Environmental Sciences, vol. 65. Springer, Dordrecht, The Netherlands, pp. 141–156.
Lombardi, S., Pinti, D.L., Rossi, U., Fiordalisi, A., 1993. ^{222}Rn in soil gases at Latera geothermal field: a preliminary case history. Geologica Romana 29, 391–399.
Minissale, A., 2004. Origin, transport and discharge of CO_2 in central Italy. Earth-Science Reviews 66, 89–141.
Morley, C.K., Wonganan, J.K., 2000. Normal fault displacement characteristics, with particular reference to synthetic transfer zones: Mae Moh mine, northern Thailand. Basin Research 12, 307–327.
Morrow, C.A., Shi, L.Q., Byerlee, J.D., 1984. Permeability of fault gouge under confining pressure and shear stress. Journal of Geophysical Research 89, 3193–3200.
Nappi, G., 1969. Genesi ed evoluzione della Caldera di Latera. Bullettino del Servizio Geologico d'Italia 90, 61–68.
Nappi, G., Renzulli, A., Santi, P., 1991. Evidence of incremental growth in the Vulsinian calderas (central Italy). Journal of Volcanology and Geochemical Research 47, 13–31.
Nicoletti, M., Petrucciani, C., Piro, M., Trigila, R., 1979. Nuove datazioni vulsine per uno schema di evoluzione dell'attività vulcanica: il quadrante nord-occidentale. Periodico di Mineralogia 47/48, 153–165.
Oldenburg, C.M., Unger, A.J.A., 2004. Coupled vadose zone and atmospheric surface layer transport of carbon dioxide from geologic carbon sequestration sites. Vadose Zone Journal 3, 848–857.
Palladino, D.M., Agosta, E., 1997. Pumice fall deposits of the Western Vulsini Volcanoes (central Italy). Volcanology and Geothermal Research 78, 77–102.
Palladino, D.M., Simei, S., 2005. The Latera Volcanic Complex (Vulsini, central Italy): eruptive activity and caldera evolution. Acta Vulcanologica 17, 75–80.
Palladino, D.M., Valentine, G.A., 1995. Coarse-tail vertical and lateral grading in pyroclastic flow deposits of the Latera Volcanic Complex (Vulsini, Central Italy): origin and implications for flow dynamics. Journal of Volcanology and Geochemical Research 69, 343–364.

Pearce, J.M. (Ed.), 2004. Natural analogues for the geological storage of CO_2. Final report of the Nascent project. British Geological Survey Technical Report, 122 pp.

Pearce, J.M., 2006. What can we learn from natural analogues? In: Lombardi, S., Altunina, L.K., Beaubien, S.E. (Eds.), Advances in the Geological Storage of Carbon Dioxide. NATO Science Series, IV. Earth and Environmental Sciences, vol. 65. Springer, pp. 129–140.

Pettinelli, E., Beaubien, S.E., Lombardi, S., Annan, A.P., 2008. GPR, TDR, and geochemistry measurements above an active gas vent to study near-surface gas-migration pathways. Geophysics 73 (1), doi:10.1190/1.2815991.

Pfanz, H., Vodnik, D., Wittmann, C., Aschan, G., Batic, F., Turk, B., Macek, I., 2007. Photosynthetic performance (CO_2-compensation point, carboxylation efficiency, and net photosynthesis) of timothy grass (*Phleum pratense* L.) is affected by elevated carbon dioxide in post-volcanic mofette areas. Environmental and Experimental Botany 61, 41–48.

Rawling, G.C., Goodwin, B.L., Wilson, J.L., 2001. Internal architecture, permeability structure, and hydrologic significance of contrasting fault-zone types. Geology 29 (1), 43–46.

Risk, D., Kellman, L., Beltrami, H., 2002. Soil CO_2 production and surface flux at four climate observatories in eastern Canada. Global Biogeochemical Cycles 16, 69–80.

Sabatelli, F., Mannari, M., 1995. Latera development update. In: Proceedings World Geothermal Congress, Florence, 18–31 May 1995.

Sholtz, C.H., 1987. Wear and gouge formation in brittle faulting. Geology 15, 493–495.

Sibson, R.H., 1977. Fault rocks and fault mechanisms. Journal of the Geological Society of London 133, 191–213.

Sibson, R.H., 1996. Structural permeability of fluid-driven fault-fracture meshes. Journal of Structural Geology 18, 1031–1042.

Sibson, R.H., 2000. Fluid involvement in normal faulting. Journal of Geodynamics 29, 469–499.

Simei, S., Acocella, V., Palladino, D.M., Trigila, R., 2006. Evolution and structure of Vulsini calderas (Italy). Geophysics Research Abstracts 8 (09302).

Sparks, R.S.J., 1975. Stratigraphy and geology of the ignimbrites of Vulsini Volcano, Italy. Geologische Rundschau 64, 497–523.

Stephens, J.C., Hering, J.G., 2002. Comparative characterization of volcanic ash soils exposed to decade-long elevated carbon dioxide concentrations at Mammoth Mountain, California. Chemical Geology 186, 301–313.

Stevens, S.H., Schoell, M., Ballentine, C., Hyman, D.M., 2004. Isotopic analysis of natural CO_2 field: how long has nature stored CO_2 underground? In: The 7th Greenhouse Gas Control Technologies Conference (GHGT7), Vancouver, Canada, 5–9 September 2004.

Tellam, 1995. Hydrochemistry of the saline ground-waters of the lower Mersey Basin Permo-Triassi sandstone aquifer, UK. Journal of Hydrogeology 165, 45–84.

Trigila, R., Walker, G.P.L., 1981. The Onano spatter flow, Italy: evidence for a new ignimbrite depositional mechanism. In: IAVCEI International Volcanology Congress, New Zealand.

Turbeville, B.N., 1992. 40Ar/39Ar ages and stratigraphy of the Latera caldera, Italy. Bulletin of Volcanology 55, 110–118.

Uehara, S., Shimamoto, T., 2004. Gas permeability evolution of cataclasite and fault gouge in triaxial compression and implication for changes in fault zone permeability structure through the earthquake cycle. Tectonophysics 378, 183–195.

Vezzoli, L., Conticelli, S., Innocenti, F., Landi, P., Manetti, P., Palladino, D.M., Trigila, R., 1987. Stratigraphy of the Latera Volcanic Complex: proposals for a new nomenclature. Periodico di Mineralogia 56, 89–110.

Wang, S., Jaffe, P.R., 2004. Dissolution of a mineral phase in potable aquifers due to CO_2 releases from deep formations. Effect of dissolution kinetics. Energy Conversion and Management 45, 2833–2848.

Wells, A.W., Diehl, J.R., Bromhal, G., Strazisar, B.R., Wilson, T.H., White, C.M., 2007. The use of tracers to assess leakage from the sequestration of CO_2 in a depleted oil reservoir, New Mexico, USA. Applied Geochemistry 22, 996–1016.

Wibberley, C.A.J., Shimamoto, T., 2003. Internal structure and permeability of major strike–slip fault zones: the Median Tectonic Line in Mie Prefecture, southwest Japan. Journal of Structural Geology 25, 59–78.

Wilson, M., Monea, M. (Eds.), 2004. IEA GHG Weyburn CO_2 Monitoring and Storage Project Summary Report 2000–2004. III. Petroleum Technology Research Centre, Regina, 273 pp.

Zhang, S., Cox, S.F., 2000. Enhancement of fluid permeability during shear deformation of a synthetic mud. Journal of Structural Geology 22, 1385–1393.

Zhang, S., Tullis, T.E., 1998. The effect of fault slip on permeability and permeability anisotropy in quartz gouge. Tectonophysics 295, 41–52.

Zhu, W., Wong, T.-F., 1997. The transition from brittle faulting to cataclastic flow: permeability evolution. Journal of Geophysical Research 102, 3027–3041.

Zhu, W., Wong, T.-F., 1999. Network modeling of the evolution of permeability and dilatancy in compact rock. Journal of Geophysical Research 104, 2963–2971.

Zoback, M.A., Byerlee, J.D., 1975. The effect of microcrack dilatancy on the permeability of Westerly granite. Journal of Geophysical Research 80, 752–755.